arXiv:1705.08883v3 [cs.CE] 5 Nov 2017

Modeling flow in porous media with double porosity/permeability

A stabilized mixed formulation, error analysis, and numerical solutions

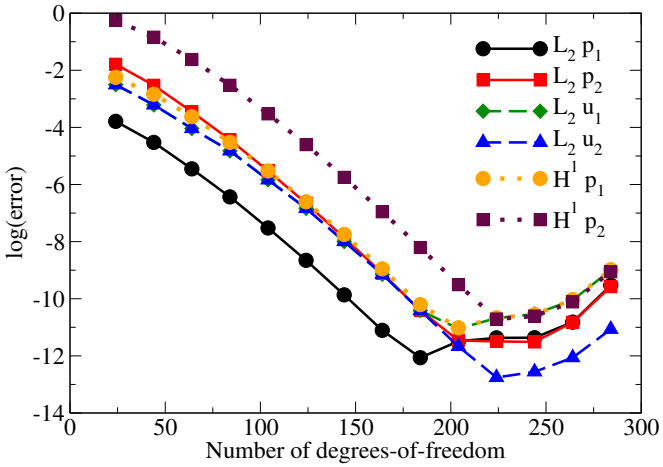
An e-print of the paper is available on arXiv: 1705/08883.

Authored by

S. H. S. Joodat
Graduate Student, University of Houston

K. B. Nakshatrala
Department of Civil & Environmental Engineering
University of Houston, Houston, Texas 77204–4003
phone: *+1-713-743-4418,* ***e-mail:*** *knakshatrala@uh.edu*
website: *http://www.cive.uh.edu/faculty/nakshatrala*

R. Ballarini
Thomas and Laura Hsu Professor and Chair
Department of Civil and Environmental Engineering, University of Houston.



This figure shows that the rates of convergence under the proposed stabilized mixed formulation is exponential with respect to p-refinement, which is in accordance with the theory.

2017
Computational & Applied Mechanics Laboratory

Modeling flow in porous media with double porosity/permeability: A stabilized mixed formulation, error analysis, and numerical solutions

S. H. S. Joodat, **K. B. Nakshatrala**, and **R. Ballarini**
Department of Civil and Environmental Engineering, University of Houston.
Correspondence to: knakshatrala@uh.edu

Abstract. The flow of incompressible fluids through porous media plays a crucial role in many technological applications such as enhanced oil recovery and geological carbon-dioxide sequestration. The flow within numerous natural and synthetic porous materials that contain multiple scales of pores cannot be adequately described by the classical Darcy equations. It is for this reason that mathematical models for fluid flow in media with multiple scales of pores have been proposed in the literature. However, these models are analytically intractable for realistic problems. In this paper, a stabilized mixed four-field finite element formulation is presented to study the flow of an incompressible fluid in porous media exhibiting double porosity/permeability. The stabilization terms and the stabilization parameters are derived in a mathematically consistent manner, and the computationally convenient equal-order interpolation of all the field variables is shown to be stable. A systematic error analysis is performed on the resulting stabilized weak formulation. Representative problems, patch tests and numerical convergence analyses are performed to illustrate the performance and convergence behavior of the proposed mixed formulation in the discrete setting. The accuracy of numerical solutions is assessed using the mathematical properties satisfied by the solutions of this double porosity/permeability model. Moreover, it is shown that the proposed framework can perform well under transient conditions and that it can capture well-known instabilities such as viscous fingering.

1. INTRODUCTION

Fluid flow in porous media has been extensively studied, both theoretically and computationally, because of its broad applications in different branches of science and engineering. The most popular model of flow of an incompressible fluid in rigid porous media is the Darcy model, which is based on the assumption that the domain contains only one pore-network. Due to the restricting assumptions in the classical Darcy model [Chang et al., 2017; Nakshatrala and Rajagopal, 2011; Rajagopal, 2007], its application has been limited and several modifications and alternative models have been proposed that predict more realistic flow behaviors. In particular, due to the complexity of the pore-structure in many geo-materials such as shale, many studies have focused on developing mathematical models and computational frameworks that consider the presence of two (or more) dominant pore-networks exhibiting different hydro-mechanical properties. Some of the recent studies on multiple pore-networks include [Borja and Koliji, 2009; Choo et al., 2015].

Key words and phrases. stabilized mixed formulations; error estimates; patch tests; double porosity/permeability; flow through porous media.

The mathematical models pertaining to the flow in porous media with multiple pore-networks are complex and involve numerous field variables. It is not always possible to derive analytical solutions to these mathematical models, and one has to resort to numerical solutions for realistic problems. Different approaches are available for developing formulations for multi-field mathematical models. Mixed finite element formulations, which offer the flexibility of using different approximations for different field variables, are particularly attractive for multi-field problems. Accurate numerical solutions have been obtained using mixed finite element for various porous media models; for example, see [Badia and Codina, 2010; Choo and Borja, 2015; Masud and Hughes, 2002; Nakshatrala and Rajagopal, 2011; Nakshatrala et al., 2006]. Moreover, many of the mathematical models pertaining to the multiple pore-networks, and in particular, the mathematical model considered in this paper, cannot be written in terms of a single-field variable. Although mixed methods are considered a powerful tool, especially for modeling flow problems in porous media, they suffer from some restrictions. To obtain stable and convergent solutions, a mixed formulation should satisfy the Ladyzhenskaya-Babuška-Brezzi (LBB) stability condition [Babuška, 1973; Brezzi and Fortin, 1991]. Numerical instability of the solution and probable spurious oscillations in the profile of unknown variables are the main consequences of the violation of this condition. Such drawbacks are observed in many of the existing formulations and highlight the need for developing more robust computational frameworks. In order to resolve numerical instabilities resulting from violation of the LBB condition, computational approaches are divided broadly into two classes [Franca and Hughes, 1988]: those that satisfy the LBB condition and those that circumvent it.

In the former approach, elements are developed by placing restrictions on the interpolation spaces so as to satisfy the LBB condition under the classical mixed (Galerkin) formulation. Such elements are collectively referred to as the H(div) elements [Brezzi and Fortin, 1991; Brezzi et al., 2008]. Two popular works of this type are Raviart-Thomas (RT) spaces [Raviart and Thomas, 1977], and Brezzi-Douglas-Marini (BDM) spaces [Brezzi et al., 1985, 1987]. The class of stabilized methods, which falls under the latter approach, is an attractive way of circumventing the LBB condition. In a stabilized formulation, stabilization terms are augmented to the classical mixed formulation to avoid a saddle-point problem as well as mathematical instabilities [Hughes et al., 2004]. Various stabilized formulations have been published for flow problems (e.g., see [Badia and Codina, 2009; Brooks and Hughes, 1982; Hughes et al., 2000; Turner et al., 2009]) and for flow problems in porous media, in particular, (e.g., see [Badia and Codina, 2010; Choo and Borja, 2015; Masud and Hughes, 2002; Nakshatrala et al., 2006]).

Herein, we develop a stabilized mixed formulation of the double porosity/permeability model proposed by [Nakshatrala et al., 2016]. The stabilization terms and the stabilization parameter are derived in a mathematically consistent manner by appealing to the variational multiscale formalism [Hughes, 1995]. It is noteworthy that the nodal-based equal-order interpolation for all the field variables is stable under the proposed stabilized mixed formulation. Such a feature for interpolations is particularly desirable for studies in porous media for two reasons. The obvious reason is that the equal-order interpolation is computationally the most convenient. The second reason is that, in many porous media applications, the flow and transport equations are coupled (Section 9 of this paper deals with such a coupled problem). But many existing formulations (including the stabilized formulations) produce non-physical negative solutions for the transport equations (i.e., a negative value for concentration fields), especially when the diffusion/dispersion is anisotropic [Nagarajan and Nakshatrala, 2011]. The known robust non-negative finite element based formulations for the

transport equations are nodal-based (e.g., refer to [Mudunuru and Nakshatrala, 2016; Nagarajan and Nakshatrala, 2011]). By choosing nodal-based unknowns even for the flow problem, one can avoid projections from nodal to non-nodal interpolation spaces and vice-versa.

To determine whether a computational framework is robust, systematic convergence and error analyses are required. To this end, we first perform a mathematically rigorous stability analysis of the proposed stabilized mixed formulation. Since the proposed formulation is residual-based, consistency is shown quite easily. We also present patch tests and representative numerical results to show that the obtained numerical results are stable. After establishing the stability of the proposed formulation, we perform a thorough accuracy assessment of the approximations by estimating the error associated with the numerical solutions. Specifically, we perform both *a priori* and *a posteriori* error estimations, which individually serve different purposes [Babuška et al., 2010]. *A posteriori* error estimations monitor different forms of the error in the numerical solution [Babuška and Strouboulis, 2001; Becker and Rannacher, 2001] and using the computed approximate solution, they provide an estimate of the form $\|u - u_h\| \leq \epsilon$, where u is the solution, u_h is the finite element solution for a mesh with mesh size h, $\|\cdot\|$ denotes an appropriate norm, and ϵ is a constant (real) number. On the other hand, *a priori* error estimations provide us with the order of convergence of a given finite element method [Ainsworth and Oden, 1997].

[Shabouei and Nakshatrala, 2016] have shown that porous media models such as those defined by the Darcy and Darcy-Brinkman equations satisfy certain mechanics-based properties, and they have utilized these properties to construct solution verification procedures. Recently, [Nakshatrala et al., 2016] have shown that the double porosity/permeability model also enjoys properties with strong mechanics underpinning. These include the minimum dissipation theorem and a reciprocal relation. Herein, we utilize these mechanics-based properties to construct *a posteriori* solution verification procedures to assess the accuracy of numerical solutions obtained under the proposed formulation for the double porosity/permeability model.

Another type of numerical instability, known as Gibbs phenomenon, can also be observed in the numerical solutions of problems associated with flow through porous media with disparate properties. In layered porous domains, conventional continuous finite element methods are not capable of capturing abrupt changes in material properties and result in overshoots and undershoots in the profiles of numerical solutions along the interface of layers where there are jump discontinuities. In order to eliminate such erroneous oscillations, one possible approach is discontinuous Galerkin (DG) methods. DG methods have been successfully employed by [Hughes et al., 2006] for the case of Darcy equations. An extension of the proposed framework using discontinuous Galerkin method for double porosity/permeability model can be obtained using a method similar to the one proposed by [Hughes et al., 2006]. However, obtaining such an extension and comparison between the performance of continuous and discontinuous formulations for capturing abrupt changes in material properties are beyond the scope of this paper and will be addressed in a subsequent one.

A common assumption in models of flow in porous media is that of steady-state conditions. However, many flows occurring in porous media such as aquifers and oil-bearing strata are transient or unsteady in nature. In this paper, we extend the proposed stabilized mixed formulation for the double porosity/permeability mathematical model to the transient case, and we illustrate this extension can accurately capture the transient flow characteristics.

Recently, it has been shown that some stabilized methods (which are primarily designed to suppress numerical instabilities) when applied to solve problems with physical instabilities, suppress

both types of instabilities [Shabouei, 2016; Shabouei and Nakshatrala]. Therefore, a good test of the proposed stabilized mixed formulation for a coupled flow and transport problem involves a problem that exhibits a physical instability similar to the classical Saffman-Taylor instability [Saffman and Taylor, 1958]. Using numerical simulations we show that the proposed formulation suppresses only the spurious numerical instabilities while capturing the underlying physical instability.

The rest of this paper is organized as follows. After an outline of the governing equations of the double porosity/permeability model in Section 2, the corresponding stabilized mixed formulation is presented in Section 3 with a derivation provided in Appendix A. The theoretical convergence analysis for the proposed stabilized mixed formulation is presented in Section 4, followed by the numerical convergence behavior of the elements presented in Section 5 where patch tests in one- and three-dimensional spaces are described. The representative numerical results are used to showcase the performance of the proposed mixed formulation in Section 6. Section 7 provides the mechanics-based assessment of the numerical accuracy. The transient analysis and the capability of the computational framework for modeling coupled problems and capturing well-known physical instabilities in fluid mechanics are discussed in Sections 8 and 9. Finally, conclusions are drawn in Section 10.

Throughout this paper, repeated indices do not imply summation. The terms *classical mixed formulation* and *Galerkin formulation* are used interchangeably.

2. GOVERNING EQUATIONS FOR DOUBLE POROSITY/PERMEABILITY

For convenience to the reader and for future referencing, we document the equations that govern the double porosity/permeability mathematical model considered in [Nakshatrala et al., 2016]. Let $\Omega \subset \mathbb{R}^{nd}$ be a bounded domain, where "nd" denotes the number of spatial dimensions. The boundary of the domain $\partial\Omega$ is assumed to be piecewise smooth. Mathematically, $\partial\Omega \equiv \overline{\Omega} - \Omega$, where the superposed bar denotes the set closure [Evans, 1998]. A spatial point is denoted by $\mathbf{x} \in \overline{\Omega}$. The gradient and divergence operators with respect to $\mathbf{x}$ are denoted by grad$[\cdot]$ and div$[\cdot]$, respectively. The unit outward normal to the boundary is denoted by $\widehat{\mathbf{n}}(\mathbf{x})$.

The porous domain is assumed to consist of two dominant pore-networks, which will be referred to as the macro-pore and micro-pore networks and are, respectively, denoted by subscripts 1 and 2. These pore-networks are connected with the possibility of mass exchange between them. The pressure field and the discharge (or Darcy) velocity in the macro-pore network are, respectively, denoted by $p_1(\mathbf{x})$ and $\mathbf{u}_1(\mathbf{x})$, and the corresponding ones in the micro-pore network are denoted by $p_2(\mathbf{x})$ and $\mathbf{u}_2(\mathbf{x})$. The governing equations under the double porosity/permeability model take the following form:

$$\mu \mathbf{K}_1^{-1}\mathbf{u}_1(\mathbf{x}) + \text{grad}[p_1] = \gamma \mathbf{b}(\mathbf{x}) \quad \text{in } \Omega \tag{2.1a}$$

$$\mu \mathbf{K}_2^{-1}\mathbf{u}_2(\mathbf{x}) + \text{grad}[p_2] = \gamma \mathbf{b}(\mathbf{x}) \quad \text{in } \Omega \tag{2.1b}$$

$$\text{div}[\mathbf{u}_1] = +\chi(\mathbf{x}) \quad \text{in } \Omega \tag{2.1c}$$

$$\text{div}[\mathbf{u}_2] = -\chi(\mathbf{x}) \quad \text{in } \Omega \tag{2.1d}$$

$$\mathbf{u}_1(\mathbf{x}) \cdot \widehat{\mathbf{n}}(\mathbf{x}) = u_{n1}(\mathbf{x}) \quad \text{on } \Gamma_1^u \tag{2.1e}$$

$$\mathbf{u}_2(\mathbf{x}) \cdot \widehat{\mathbf{n}}(\mathbf{x}) = u_{n2}(\mathbf{x}) \quad \text{on } \Gamma_2^u \tag{2.1f}$$

$$p_1(\mathbf{x}) = p_{01}(\mathbf{x}) \quad \text{on } \Gamma_1^p \tag{2.1g}$$

$$p_2(\mathbf{x}) = p_{02}(\mathbf{x}) \quad \text{on } \Gamma_2^p \tag{2.1h}$$

where $\mathbf{b}(\mathbf{x})$ is the specific body force. The true density and coefficient of viscosity of the fluid are, respectively, denoted by γ and μ. $\mathbf{K}_i(\mathbf{x})$ denotes the permeability tensor for macro-pore ($i = 1$) and micro-pore ($i = 2$) networks. Γ_i^u denotes the part of the boundary on which the normal component of the velocity is prescribed in the macro-pore ($i = 1$) and micro-pore ($i = 2$) networks. Similarly, Γ_i^p is that part of the boundary on which the pressure is prescribed in the macro-pore ($i = 1$) and micro-pore ($i = 2$) networks. $p_{01}(\mathbf{x})$ and $p_{02}(\mathbf{x})$ denote the prescribed pressures on Γ_1^p and Γ_2^p, respectively. $u_{n1}(\mathbf{x})$ and $u_{n2}(\mathbf{x})$ denote the prescribed normal components of the velocities on Γ_1^u and Γ_2^u, respectively. $\chi(\mathbf{x})$ is the rate of volume exchange of the fluid between the two pore-networks per unit volume of the porous medium, and we model it as follows [Barenblatt et al., 1960]:

$$\chi(\mathbf{x}) = -\frac{\beta}{\mu}(p_1(\mathbf{x}) - p_2(\mathbf{x})) \tag{2.2}$$

where β is a dimensionless characteristic of the porous medium. In the rest of the paper, as is commonly done in the literature, $\chi(\mathbf{x})$ will be simply referred to as the mass transfer. For mathematical well-posedness, we assume that

$$\Gamma_1^u \cup \Gamma_1^p = \partial\Omega, \quad \Gamma_1^u \cap \Gamma_1^p = \emptyset, \quad \Gamma_2^u \cup \Gamma_2^p = \partial\Omega \quad \text{and} \quad \Gamma_2^u \cap \Gamma_2^p = \emptyset \tag{2.3}$$

3. A STABILIZED MIXED WEAK FORMULATION

In this section, we present the proposed stabilized mixed formulation for the double porosity/permeability model. A derivation of the proposed formulation is provided in Appendix A. The proposed formulation is built upon the stabilization ideas put forth in a pioneering paper by [Masud and Hughes, 2002]. The proposed formulation for double porosity/permeability model can be obtained by adding a stabilization term, similar to the one proposed by [Masud and Hughes, 2002] for the case of single-pore network Darcy equations, to each pore-network. The stabilization terms are based on the residual of the balance of linear momentum in each pore-network. The stability can be achieved without adding residual-based stabilization terms related to the mass balance equations for any of the pore-networks. We also present an extension of the proposed formulation for enforcing the velocity boundary conditions weakly, which will be convenient for problems involving curved boundaries. This extension is achieved by employing a procedure similar to the one proposed by [Nitsche, 1971].

We define the relevant function spaces, which will be used in the rest of this paper. We denote the set of all square-integrable functions on Ω by $L_2(\Omega)$. For mathematical well-posedness, we assume that

$$\gamma\mathbf{b}(\mathbf{x}) \in (L_2(\Omega))^{nd},\ p_{01}(\mathbf{x}) \in H^{1/2}(\Gamma_1^p) \quad \text{and} \quad p_{02}(\mathbf{x}) \in H^{1/2}(\Gamma_2^p) \tag{3.1}$$

where $H^{1/2}(\cdot)$ is a non-integer Sobolev space [Adams and Fournier, 2003]. The function spaces for the velocity and pressures fields are defined as follows:

$$\mathcal{U}_1 := \left\{ \mathbf{u}_1(\mathbf{x}) \in (L_2(\Omega))^{nd} \;\middle|\; \mathrm{div}[\mathbf{u}_1] \in L_2(\Omega), \mathbf{u}_1(\mathbf{x}) \cdot \widehat{\mathbf{n}}(\mathbf{x}) = u_{n1}(\mathbf{x}) \in H^{-1/2}(\Gamma_1^u) \right\} \tag{3.2a}$$

$$\mathcal{U}_2 := \left\{ \mathbf{u}_2(\mathbf{x}) \in (L_2(\Omega))^{nd} \;\middle|\; \mathrm{div}[\mathbf{u}_2] \in L_2(\Omega), \mathbf{u}_2(\mathbf{x}) \cdot \widehat{\mathbf{n}}(\mathbf{x}) = u_{n2}(\mathbf{x}) \in H^{-1/2}(\Gamma_2^u) \right\} \tag{3.2b}$$

$$\mathcal{W}_1 := \left\{ \mathbf{w}_1(\mathbf{x}) \in (L_2(\Omega))^{nd} \;\middle|\; \mathrm{div}[\mathbf{w}_1] \in L_2(\Omega), \mathbf{w}_1(\mathbf{x}) \cdot \widehat{\mathbf{n}}(\mathbf{x}) = 0 \text{ on } \Gamma_1^u \right\} \tag{3.2c}$$

$$\mathcal{W}_2 := \left\{ \mathbf{w}_2(\mathbf{x}) \in (L_2(\Omega))^{nd} \;\middle|\; \mathrm{div}[\mathbf{w}_2] \in L_2(\Omega), \mathbf{w}_2(\mathbf{x}) \cdot \widehat{\mathbf{n}}(\mathbf{x}) = 0 \text{ on } \Gamma_2^u \right\} \tag{3.2d}$$

$$\mathcal{P} := \left\{ (p_1(\mathbf{x}), p_2(\mathbf{x})) \in L_2(\Omega) \times L_2(\Omega) \;\middle|\; \left(\int_\Omega p_1(\mathbf{x}) \mathrm{d}\Omega\right)\left(\int_\Omega p_2(\mathbf{x}) \mathrm{d}\Omega\right) = 0 \right\} \tag{3.2e}$$

$$\mathcal{Q} := \left\{ (p_1(\mathbf{x}), p_2(\mathbf{x})) \in H^1(\Omega) \times H^1(\Omega) \;\middle|\; \left(\int_\Omega p_1(\mathbf{x}) \mathrm{d}\Omega\right)\left(\int_\Omega p_2(\mathbf{x}) \mathrm{d}\Omega\right) = 0 \right\} \tag{3.2f}$$

where $H^1(\Omega)$ is a standard Sobolev space, and $H^{-1/2}(\cdot)$ is the dual space corresponding to $H^{1/2}(\cdot)$ [Adams and Fournier, 2003]. The standard L_2 inner-product over a set K is denoted as

$$(\mathbf{a}; \mathbf{b})_K \equiv \int_K \mathbf{a}(\mathbf{x}) \cdot \mathbf{b}(\mathbf{x}) \, \mathrm{d}K \tag{3.3}$$

For convenience, the subscript K will be dropped if $K = \Omega$. Moreover, the action of a linear functional on a vector from its associated vector space is denoted by $\langle \cdot; \cdot \rangle$.

A few remarks are needed regarding the following condition on the pressures in the function spaces $\mathcal{P}$ and $\mathcal{Q}$:

$$\left(\int_\Omega p_1(\mathbf{x}) \mathrm{d}\Omega\right)\left(\int_\Omega p_2(\mathbf{x}) \mathrm{d}\Omega\right) = 0$$

This condition of vanishing mean pressure in one of pore-networks is a mathematically elegant way of fixing the datum for the pressure. Without fixing the datum for the pressure (which will be the case when only the velocity boundary conditions are prescribed on the entire boundary), one can find the pressures only up to an arbitrary constant, which will be the case even under Darcy equations [Nakshatrala et al., 2006]. Herein, we introduced the vanishing mean pressure condition into the function spaces to ensure uniqueness of the solutions, which will be established later in this paper. However, it should be emphasized that vanishing mean pressure in one of the pore-networks is *not* necessary for all the problems under the double porosity/permeability model. One can fix the datum for the pressure under the double porosity/permeability model by prescribing the pressure in at least one of the pore-networks on a portion of the boundary, which is a set of non-zero measure. To put it differently, for problems with pressure boundary conditions, the datum for the pressure is automatically fixed through the prescribed boundary condition, and hence, for those problems, one does not include the zero mean pressure condition in the function spaces $\mathcal{P}$ and $\mathcal{Q}$. For example, see the problem in subsection 5.1, which deals with prescribed pressure boundary conditions.

The *classical mixed formulation*, which is based on the Galerkin formalism, reads as follows: Find $(\mathbf{u}_1(\mathbf{x}), \mathbf{u}_2(\mathbf{x})) \in \mathcal{U}_1 \times \mathcal{U}_2$ and $(p_1(\mathbf{x}), p_2(\mathbf{x})) \in \mathcal{P}$ such that we have

$$\begin{aligned} &\mathcal{B}_{\text{Gal}}(\mathbf{w}_1, \mathbf{w}_2, q_1, q_2; \mathbf{u}_1, \mathbf{u}_2, p_1, p_2) = \mathcal{L}_{\text{Gal}}(\mathbf{w}_1, \mathbf{w}_2, q_1, q_2) \\ &\qquad \forall \, (\mathbf{w}_1(\mathbf{x}), \mathbf{w}_2(\mathbf{x})) \in \mathcal{W}_1 \times \mathcal{W}_2, \;\; (q_1(\mathbf{x}), \;\; q_2(\mathbf{x})) \in \mathcal{P} \end{aligned} \tag{3.4}$$

where the bilinear form and the linear functional are, respectively, defined as follows:

$$\begin{aligned} \mathcal{B}_{\text{Gal}}(\mathbf{w}_1, \mathbf{w}_2, q_1, q_2; \mathbf{u}_1, \mathbf{u}_2, p_1, p_2) := \; & (\mathbf{w}_1; \mu \mathbf{K}_1^{-1} \mathbf{u}_1) - (\text{div}[\mathbf{w}_1]; p_1) + (q_1; \text{div}[\mathbf{u}_1]) \\ & + (\mathbf{w}_2; \mu \mathbf{K}_2^{-1} \mathbf{u}_2) - (\text{div}[\mathbf{w}_2]; p_2) + (q_2; \text{div}[\mathbf{u}_2]) \\ & + (q_1 - q_2; \beta/\mu (p_1 - p_2)) \end{aligned} \tag{3.5}$$

$$\mathcal{L}_{\text{Gal}}(\mathbf{w}_1, \mathbf{w}_2, q_1, q_2) := (\mathbf{w}_1; \gamma \mathbf{b}) \; + (\mathbf{w}_2; \gamma \mathbf{b}) - \langle \mathbf{w}_1 \cdot \widehat{\mathbf{n}}; p_{01} \rangle_{\Gamma_1^{\text{p}}} - \langle \mathbf{w}_2 \cdot \widehat{\mathbf{n}}; p_{02} \rangle_{\Gamma_2^{\text{p}}} \tag{3.6}$$

In a subsequent section, we will show that the equal-order interpolation for all the variables, which is computationally the most convenient, is not stable under the classical mixed formulation. Of course, one could use divergence-free elements (e.g., Raviart-Thomas spaces [Raviart and

Thomas, 1977]) but they need special data structures and computer implementations. We, therefore, present a stabilized mixed formulation, which is stable under the equal-order interpolation for all the field variables.

The *proposed stabilized mixed formulation* reads as follows: Find $(\mathbf{u}_1(\mathbf{x}), \mathbf{u}_2(\mathbf{x})) \in \mathcal{U}_1 \times \mathcal{U}_2$ and $(p_1(\mathbf{x}), p_2(\mathbf{x})) \in \mathcal{Q}$ such that we have

$$\begin{aligned} \mathcal{B}_{\text{stab}}(\mathbf{w}_1, \mathbf{w}_2, q_1, q_2; \mathbf{u}_1, \mathbf{u}_2, p_1, p_2) &= \mathcal{L}_{\text{stab}}(\mathbf{w}_1, \mathbf{w}_2, q_1, q_2) \\ \forall\, (\mathbf{w}_1(\mathbf{x}), \mathbf{w}_2(\mathbf{x})) \ &\in \mathcal{W}_1 \times \mathcal{W}_2, (q_1(\mathbf{x}), q_2(\mathbf{x})) \in \mathcal{Q} \end{aligned} \tag{3.7}$$

where the bilinear form and the linear functional are, respectively, defined as follows:

$$\begin{aligned} \mathcal{B}_{\text{stab}}(\mathbf{w}_1, \mathbf{w}_2, q_1, q_2; \mathbf{u}_1, \mathbf{u}_2, p_1, p_2) &:= \mathcal{B}_{\text{Gal}}(\mathbf{w}_1, \mathbf{w}_2, q_1, q_2; \mathbf{u}_1, \mathbf{u}_2, p_1, p_2) \\ &- \frac{1}{2}\left(\mu \mathbf{K}_1^{-1}\mathbf{w}_1 - \text{grad}[q_1]; \frac{1}{\mu}\mathbf{K}_1(\mu \mathbf{K}_1^{-1}\mathbf{u}_1 + \text{grad}[p_1])\right) \\ &- \frac{1}{2}\left(\mu \mathbf{K}_2^{-1}\mathbf{w}_2 - \text{grad}[q_2]; \frac{1}{\mu}\mathbf{K}_2(\mu \mathbf{K}_2^{-1}\mathbf{u}_2 + \text{grad}[p_2])\right) \end{aligned} \tag{3.8}$$

$$\begin{aligned} \mathcal{L}_{\text{stab}}(\mathbf{w}_1, \mathbf{w}_2, q_1, q_2) &:= \mathcal{L}_{\text{Gal}}(\mathbf{w}_1, \mathbf{w}_2, q_1, q_2) - \frac{1}{2}\left(\mu \mathbf{K}_1^{-1}\mathbf{w}_1 - \text{grad}[q_1]; \frac{1}{\mu}\mathbf{K}_1\gamma\mathbf{b}\right) \\ &- \frac{1}{2}\left(\mu \mathbf{K}_2^{-1}\mathbf{w}_2 - \text{grad}[q_2]; \frac{1}{\mu}\mathbf{K}_2\gamma\mathbf{b}\right) \end{aligned} \tag{3.9}$$

In subsequent sections, we show that the proposed stabilized mixed formulation is consistent, stable and accurate.

3.1. Weak enforcement of velocity boundary conditions. In the previous derivations made earlier in this section, the pressure boundary conditions (i.e., equations (2.1g) and (2.1h)) are enforced weakly under the proposed stabilized mixed formulation and the classical mixed formulation. However, the velocity boundary conditions in which the normal components of the velocities are prescribed (i.e., equations (2.1e) and (2.1f)) are enforced strongly. For domains with curved boundaries, which are commonly encountered in subsurface modeling, it is desirable to even prescribe the velocity boundary conditions weakly. We, therefore, provide a possible extension of the proposed stabilized mixed formulation for weak enforcement of the velocity boundary conditions. To this end, we follow the approach proposed by [Nitsche, 1971]. The Nitsche's method is a powerful tool for weakly enforcing Dirichlet boundary conditions without the use of Lagrange multipliers, and has been utilized by several works such as [Annavarapu et al., 2014; Bazilevs and Hughes, 2007; Embar et al., 2010; Schillinger et al., 2016]. The Nitsche's method is sometimes referred to as a variationally consistent penalty method to enforce Dirichlet boundary conditions [Hansbo, 2005]. We extend the Nitsche's method to the proposed four-field stabilized formulation to enforce the prescribed normal components of the velocities in the macro- and micro-pore networks.

The stabilized mixed formulation that enforces the velocity boundary conditions weakly can be obtained as follows: Find $(\mathbf{u}_1(\mathbf{x}), \mathbf{u}_2(\mathbf{x})) \in H(\text{div}, \Omega) \times H(\text{div}, \Omega)$ and $(p_1(\mathbf{x}), p_2(\mathbf{x})) \in \mathcal{Q}$ such that we have

$$\begin{aligned} \mathcal{B}_{\text{stab}}^{\text{weak B.C.}}(\mathbf{w}_1, \mathbf{w}_2, q_1, q_2; \mathbf{u}_1, \mathbf{u}_2, p_1, p_2) &= \mathcal{L}_{\text{stab}}^{\text{weak B.C.}}(\mathbf{w}_1, \mathbf{w}_2, q_1, q_2) \\ \forall\, (\mathbf{w}_1(\mathbf{x}), \mathbf{w}_2(\mathbf{x})) \ &\in H(\text{div}, \Omega) \times H(\text{div}, \Omega),\ (q_1(\mathbf{x}), q_2(\mathbf{x})) \in \mathcal{Q} \end{aligned} \tag{3.10}$$

where the bilinear form and the linear functional are, respectively, defined as follows:

$$\begin{aligned}\mathcal{B}_{\text{stab}}^{\text{weak B.C.}}(\mathbf{w}_1,\mathbf{w}_2,q_1,q_2;\mathbf{u}_1,\mathbf{u}_2,p_1,p_2) &:= \mathcal{B}_{\text{stab}}(\mathbf{w}_1,\mathbf{w}_2,q_1,q_2;\mathbf{u}_1,\mathbf{u}_2,p_1,p_2)\\ &+ (\mathbf{w}_1\cdot\widehat{\mathbf{n}};p_1)_{\Gamma_1^u} + (\mathbf{w}_2\cdot\widehat{\mathbf{n}};p_2)_{\Gamma_2^u}\\ &+ (q_1;\mathbf{u}_1\cdot\widehat{\mathbf{n}})_{\Gamma_1^u} + (q_2;\mathbf{u}_2\cdot\widehat{\mathbf{n}})_{\Gamma_2^u}\\ &+ \frac{\eta}{h}(\mathbf{w}_1\cdot\widehat{\mathbf{n}};\mathbf{u}_1\cdot\widehat{\mathbf{n}})_{\Gamma_1^u} + \frac{\eta}{h}(\mathbf{w}_2\cdot\widehat{\mathbf{n}};\mathbf{u}_2\cdot\widehat{\mathbf{n}})_{\Gamma_2^u} \qquad (3.11a)\end{aligned}$$

$$\begin{aligned}\mathcal{L}_{\text{stab}}^{\text{weak B.C.}}(\mathbf{w}_1,\mathbf{w}_2,q_1,q_2) &:= \mathcal{L}_{\text{stab}}(\mathbf{w}_1,\mathbf{w}_2,q_1,q_2) + (q_1;u_{n1})_{\Gamma_1^u} + (q_2;u_{n2})_{\Gamma_2^u}\\ &+ \frac{\eta}{h}(\mathbf{w}_1\cdot\widehat{\mathbf{n}};u_{n1})_{\Gamma_1^u} + \frac{\eta}{h}(\mathbf{w}_2\cdot\widehat{\mathbf{n}};u_{n2})_{\Gamma_2^u} \qquad (3.11b)\end{aligned}$$

where h is the mesh size and η is the penalty parameter. In this paper, we have taken h to be the maximum edge length in the mesh, and have taken the penalty parameter to be 10. In the above statement of the weak formulation, since the velocity boundary conditions are enforced weakly, the appropriate function space for the velocities and the associated weighting functions will be $H(\text{div},\Omega)$, which can be mathematically defined as follows:

$$H(\text{div},\Omega) := \left\{\mathbf{u}(\mathbf{x}) \in (L_2(\Omega))^{nd} \;\middle|\; \text{div}[\mathbf{u}] \in L_2(\Omega)\right\} \qquad (3.12)$$

The function spaces for the pressures and their weighting functions, however, remain same as before (i.e., the $\mathcal{Q}$ space).

4. A THEORETICAL ANALYSIS OF THE PROPOSED MIXED FORMULATION

In this section, we present a systematic mathematical analysis (i.e., existence, uniqueness and well-posedness) and error analysis (i.e., consistency, stability, order of convergence) of the proposed stabilized mixed formulation. For convenience, we define the following product spaces:

$$\mathbb{U} = \mathcal{U}_1 \times \mathcal{U}_2 \times \mathcal{Q}, \quad \text{and} \quad \mathbb{W} = \mathcal{W}_1 \times \mathcal{W}_2 \times \mathcal{Q} \qquad (4.1)$$

We group the field variables as follows:

$$\mathbf{U} = (\mathbf{u}_1(\mathbf{x}),\mathbf{u}_2(\mathbf{x}),p_1(\mathbf{x}),p_2(\mathbf{x})) \in \mathbb{U} \qquad (4.2a)$$

$$\mathbf{W} = (\mathbf{w}_1(\mathbf{x}),\mathbf{w}_2(\mathbf{x}),q_1(\mathbf{x}),q_2(\mathbf{x})) \in \mathbb{W} \qquad (4.2b)$$

Then, the proposed mixed formulation in equation (3.7) can be compactly written as: Find $\mathbf{U} \in \mathbb{U}$ such that we have

$$\mathcal{B}_{\text{stab}}(\mathbf{W},\mathbf{U}) = \mathcal{L}_{\text{stab}}(\mathbf{W}) \quad \forall \mathbf{W} \in \mathbb{W} \qquad (4.3)$$

We shall establish the stability of the formulation under the following norm:

$$\begin{aligned}\|\mathbf{W}\|_{\text{stab}}^2 := \mathcal{B}_{\text{stab}}(\mathbf{W},\mathbf{W}) &= \frac{1}{2}\left\|\sqrt{\mu}\mathbf{K}_1^{-1/2}\mathbf{w}_1\right\|^2 + \frac{1}{2}\left\|\frac{1}{\sqrt{\mu}}\mathbf{K}_1^{1/2}\text{grad}[q_1]\right\|^2 + \frac{1}{2}\left\|\sqrt{\mu}\mathbf{K}_2^{-1/2}\mathbf{w}_2\right\|^2\\ &+ \frac{1}{2}\left\|\frac{1}{\sqrt{\mu}}\mathbf{K}_2^{1/2}\text{grad}[q_2]\right\|^2 + \left\|\sqrt{\left(\frac{\beta}{\mu}\right)}(q_1-q_2)\right\|^2 \quad \forall \mathbf{W} \in \mathbb{W} \qquad (4.4)\end{aligned}$$

where $\|\cdot\|$ denotes the norm corresponding to the standard L_2 inner-product. We need to first show that $\|\cdot\|_{\text{stab}}$ is in fact a norm on $\mathbb{W}$ and $\mathbb{U}$. To this end, the following lemma will be used.

LEMMA 4.1. *(A property of semi-norms) If $\|\cdot\|_1$ and $\|\cdot\|_2$ are semi-norms, then $\|\cdot\|_3 := \sqrt{\|\cdot\|_1^2 + \|\cdot\|_2^2}$ is also a semi-norm.*

PROOF. The homogeneity of $\|\cdot\|_3$ directly stems from the homogeneity of the semi-norms $\|\cdot\|_1$ and $\|\cdot\|_2$. To wit,

$$\|\alpha\mathbf{x}\|_3 = \sqrt{\|\alpha\mathbf{x}\|_1^2 + \|\alpha\mathbf{x}\|_2^2} = \sqrt{|\alpha|^2\|\mathbf{x}\|_1^2 + |\alpha|^2\|\mathbf{x}\|_2^2} = |\alpha|\sqrt{\|\mathbf{x}\|_1^2 + \|\mathbf{x}\|_2^2} = |\alpha|\|\mathbf{x}\|_3 \tag{4.5}$$

The non-negativity of $\|\cdot\|_3$ is straightforward; that is, $\|\mathbf{x}\|_3 \geq 0\ \forall \mathbf{x}$. The triangle inequality for the semi-norms $\|\cdot\|_1$ and $\|\cdot\|_2$ implies that

$$\|\mathbf{a}+\mathbf{b}\|_1 \leq \|\mathbf{a}\|_1 + \|\mathbf{b}\|_1, \quad \text{and} \quad \|\mathbf{a}+\mathbf{b}\|_2 \leq \|\mathbf{a}\|_2 + \|\mathbf{b}\|_2 \tag{4.6}$$

These inequalities imply that

$$\begin{aligned}
\|\mathbf{a}+\mathbf{b}\|_3^2 &= \|\mathbf{a}+\mathbf{b}\|_1^2 + \|\mathbf{a}+\mathbf{b}\|_2^2 \\
&\leq \|\mathbf{a}\|_1^2 + \|\mathbf{a}\|_2^2 + \|\mathbf{b}\|_1^2 + \|\mathbf{b}\|_2^2 + 2\left\{\|\mathbf{a}\|_1\|\mathbf{b}\|_1 + \|\mathbf{a}\|_2\|\mathbf{b}\|_2\right\} \\
&\leq \left(\sqrt{\|\mathbf{a}\|_1^2 + \|\mathbf{a}\|_2^2}\right)^2 + \left(\sqrt{\|\mathbf{b}\|_1^2 + \|\mathbf{b}\|_2^2}\right)^2 + 2\sqrt{\|\mathbf{a}\|_1^2 + \|\mathbf{a}\|_2^2}\sqrt{\|\mathbf{b}\|_1^2 + \|\mathbf{b}\|_2^2}
\end{aligned} \tag{4.7}$$

We have employed the AM-GM inequality in obtaining equation (4.7), which further implies that

$$\|\mathbf{a}+\mathbf{b}\|_3 \leq \sqrt{\|\mathbf{a}\|_1^2 + \|\mathbf{a}\|_2^2} + \sqrt{\|\mathbf{b}\|_1^2 + \|\mathbf{b}\|_2^2} = \|\mathbf{a}\|_3 + \|\mathbf{b}\|_3 \tag{4.8}$$

This establishes the triangle inequality for $\|\cdot\|_3$. The homogeneity, non-negativity and triangle inequality imply that $\|\cdot\|_3$ is a semi-norm. □

PROPOSITION 4.1. *(Stability norm)* $\|\cdot\|_{\text{stab}}$ *is a norm on* $\mathbb{W}$ *and* $\mathbb{U}$.

PROOF. We first note that $\mathbf{K}_1$ and $\mathbf{K}_2$ are symmetric and positive definite tensors. The square root of a symmetric and positive definite tensor exists, and is itself a symmetric and positive definite tensor [Gurtin, 1981]. This implies that the following individual terms form semi-norms on $\mathbb{W}$ and $\mathbb{U}$:

$$\begin{gathered}
\frac{1}{\sqrt{2}}\left\|\sqrt{\mu}\mathbf{K}_1^{-1/2}\mathbf{w}_1\right\|, \ \frac{1}{\sqrt{2}}\left\|\frac{1}{\sqrt{\mu}}\mathbf{K}_1^{1/2}\text{grad}[q_1]\right\|, \ \frac{1}{\sqrt{2}}\left\|\sqrt{\mu}\mathbf{K}_2^{-1/2}\mathbf{w}_2\right\|, \\
\frac{1}{\sqrt{2}}\left\|\frac{1}{\sqrt{\mu}}\mathbf{K}_2^{1/2}\text{grad}[q_2]\right\|, \quad \text{and} \quad \left\|\sqrt{\left(\frac{\beta}{\mu}\right)}(q_1 - q_2)\right\|
\end{gathered} \tag{4.9}$$

Then, Lemma 4.1 implies that $\|\cdot\|_{\text{stab}}$ is a semi-norm. It is easy to show that $\|\mathbf{W}\|_{\text{stab}} = 0$ implies that

$$\mathbf{w}_1(\mathbf{x}) = \mathbf{0},\ \mathbf{w}_2(\mathbf{x}) = \mathbf{0} \text{ and } q_1(\mathbf{x}) = q_2(\mathbf{x}) = c \tag{4.10}$$

where c is a constant. Noting that $(q_1(\mathbf{x}), q_2(\mathbf{x})) \in \mathcal{Q}$ and utilizing the following condition in the definition of $\mathcal{Q}$:

$$\left(\int_\Omega q_1(\mathbf{x})\text{d}\Omega\right)\left(\int_\Omega q_2(\mathbf{x})\text{d}\Omega\right) = 0 \tag{4.11}$$

we conclude that $c = 0$. With this, we have established that $\|\mathbf{W}\|_{\text{stab}} = 0$ implies that $\mathbf{W} = \mathbf{0}$. Hence, $\|\cdot\|_{\text{stab}}$ is a norm. □

THEOREM 4.1. *(Uniqueness of weak solutions) The weak solution under the proposed mixed formulation is unique.*

PROOF. On the contrary, assume that $\mathbf{U}_1$ and $\mathbf{U}_2$ are both (weak) solutions of the weak formulation. This implies that

$$\mathcal{B}_{\text{stab}}(\mathbf{W},\mathbf{U}_1)=\mathcal{L}_{\text{stab}}(\mathbf{W}) \quad \forall \mathbf{W}\in\mathbb{W}, \quad \text{and} \quad \mathcal{B}_{\text{stab}}(\mathbf{W},\mathbf{U}_2)=\mathcal{L}_{\text{stab}}(\mathbf{W}) \quad \forall \mathbf{W}\in\mathbb{W} \tag{4.12}$$

By subtracting the above two equations and noting the linearity in the second slot, we obtain

$$\mathcal{B}_{\text{stab}}(\mathbf{W},\mathbf{U}_1-\mathbf{U}_2)=0 \quad \forall \mathbf{W}\in\mathbb{W} \tag{4.13}$$

Since $\mathbf{U}_1-\mathbf{U}_2\in\mathbb{W}$, we can choose $\mathbf{W}=\mathbf{U}_1-\mathbf{U}_2$. This particular choice implies that

$$\mathcal{B}_{\text{stab}}(\mathbf{U}_1-\mathbf{U}_2,\mathbf{U}_1-\mathbf{U}_2)=\|\mathbf{U}_1-\mathbf{U}_2\|^2_{\text{stab}}=0 \tag{4.14}$$

Using Proposition 4.1 (which establishes that $\|\cdot\|_{\text{stab}}$ is a norm on $\mathbb{W}$) we conclude that $\mathbf{U}_1=\mathbf{U}_2$. □

THEOREM 4.2. *(Boundedness) The bilinear form is bounded. That is,*

$$\Big|\mathcal{B}_{\text{stab}}(\mathbf{W},\mathbf{U})\Big|\leq C\|\mathbf{W}\|_{\text{stab}}\|\mathbf{U}\|_{\text{stab}} \tag{4.15}$$

where C is a constant.

PROOF. A direct application of the triangle inequality of the absolute value on real numbers implies that

$$\begin{aligned}\Big|\mathcal{B}_{\text{stab}}(\mathbf{W},\mathbf{U})\Big| \leq{}& \frac{1}{2}\Big|\left(\mathbf{w}_1;\mu\mathbf{K}_1^{-1}\mathbf{u}_1\right)\Big|+\frac{1}{2}\Big|\left(\mathbf{w}_2;\mu\mathbf{K}_2^{-1}\mathbf{u}_2\right)\Big|+\frac{1}{2}\Big|\left(\mathbf{w}_1;\text{grad}[p_1]\right)\Big|+\frac{1}{2}\Big|\left(\mathbf{w}_2;\text{grad}[p_2]\right)\Big|\\ &+\frac{1}{2}\Big|\left(\text{grad}[q_1];\mu^{-1}\mathbf{K}_1\text{grad}[p_1]\right)\Big|+\frac{1}{2}\Big|\left(\text{grad}[q_2];\mu^{-1}\mathbf{K}_2\text{grad}[p_2]\right)\Big|\\ &+\Big|\left(q_1-q_2;\beta/\mu(p_1-p_2)\right)\Big|\end{aligned} \tag{4.16}$$

Cauchy-Schwartz inequality on L_2 inner-product implies that

$$\begin{aligned}\Big|\mathcal{B}_{\text{stab}}(\mathbf{W},\mathbf{U})\Big| \leq{}& \frac{1}{2}\left\|\sqrt{\mu}\mathbf{K}_1^{-1/2}\mathbf{w}_1\right\|\left\|\sqrt{\mu}\mathbf{K}_1^{-1/2}\mathbf{u}_1\right\|+\frac{1}{2}\left\|\sqrt{\mu}\mathbf{K}_2^{-1/2}\mathbf{w}_2\right\|\left\|\sqrt{\mu}\mathbf{K}_2^{-1/2}\mathbf{u}_2\right\|\\ &+\frac{1}{2}\left\|\sqrt{\mu}\mathbf{K}_1^{-1/2}\mathbf{w}_1\right\|\left\|\frac{1}{\sqrt{\mu}}\mathbf{K}_1^{1/2}\text{grad}[p_1]\right\|+\frac{1}{2}\left\|\sqrt{\mu}\mathbf{K}_2^{-1/2}\mathbf{w}_2\right\|\left\|\frac{1}{\sqrt{\mu}}\mathbf{K}_2^{1/2}\text{grad}[p_2]\right\|\\ &+\frac{1}{2}\left\|\frac{1}{\sqrt{\mu}}\mathbf{K}_1^{1/2}\text{grad}[q_1]\right\|\left\|\frac{1}{\sqrt{\mu}}\mathbf{K}_1^{1/2}\text{grad}[p_1]\right\|+\frac{1}{2}\left\|\frac{1}{\sqrt{\mu}}\mathbf{K}_2^{1/2}\text{grad}[q_2]\right\|\left\|\frac{1}{\sqrt{\mu}}\mathbf{K}_2^{1/2}\text{grad}[p_2]\right\|\\ &+\left\|\sqrt{\frac{\beta}{\mu}}\left(q_1-q_2\right)\right\|\left\|\sqrt{\frac{\beta}{\mu}}\left(p_1-p_2\right)\right\|\end{aligned} \tag{4.17}$$

By applying Cauchy-Schwartz inequality on n-tuple real numbers (i.e., on Euclidean spaces) we obtained the following:

$$\begin{aligned}&\Big|\mathcal{B}_{\text{stab}}(\mathbf{W},\mathbf{U})\Big|\leq\\ &\sqrt{\left\|\sqrt{\mu}\mathbf{K}_1^{-1/2}\mathbf{w}_1\right\|^2+\left\|\sqrt{\mu}\mathbf{K}_2^{-1/2}\mathbf{w}_2\right\|^2+\frac{1}{2}\left\|\frac{1}{\sqrt{\mu}}\mathbf{K}_1^{1/2}\text{grad}[q_1]\right\|^2+\frac{1}{2}\left\|\frac{1}{\sqrt{\mu}}\mathbf{K}_2^{1/2}\text{grad}[q_2]\right\|^2+\left\|\sqrt{\frac{\beta}{\mu}}\left(q_1-q_2\right)\right\|^2}\\ &\sqrt{\frac{1}{2}\left\|\sqrt{\mu}\mathbf{K}_1^{-1/2}\mathbf{u}_1\right\|^2+\frac{1}{2}\left\|\sqrt{\mu}\mathbf{K}_2^{-1/2}\mathbf{u}_2\right\|^2+\left\|\frac{1}{\sqrt{\mu}}\mathbf{K}_1^{1/2}\text{grad}[p_1]\right\|^2+\left\|\frac{1}{\sqrt{\mu}}\mathbf{K}_2^{1/2}\text{grad}[p_2]\right\|^2+\left\|\sqrt{\frac{\beta}{\mu}}\left(p_1-p_2\right)\right\|^2}\\ &\leq 2\sqrt{\frac{1}{2}\left\|\sqrt{\mu}\mathbf{K}_1^{-1/2}\mathbf{w}_1\right\|^2+\frac{1}{2}\left\|\sqrt{\mu}\mathbf{K}_2^{-1/2}\mathbf{w}_2\right\|^2+\frac{1}{2}\left\|\frac{1}{\sqrt{\mu}}\mathbf{K}_1^{1/2}\text{grad}[q_1]\right\|^2+\frac{1}{2}\left\|\frac{1}{\sqrt{\mu}}\mathbf{K}_2^{1/2}\text{grad}[q_2]\right\|^2+\left\|\sqrt{\frac{\beta}{\mu}}\left(q_1-q_2\right)\right\|^2}\end{aligned}$$

$$\sqrt{\frac{1}{2}\left\|\sqrt{\mu}\mathbf{K}_1^{-1/2}\mathbf{u}_1\right\|^2+\frac{1}{2}\left\|\sqrt{\mu}\mathbf{K}_2^{-1/2}\mathbf{u}_2\right\|^2+\frac{1}{2}\left\|\frac{1}{\sqrt{\mu}}\mathbf{K}_1^{1/2}\mathrm{grad}[p_1]\right\|^2+\frac{1}{2}\left\|\frac{1}{\sqrt{\mu}}\mathbf{K}_2^{1/2}\mathrm{grad}[p_2]\right\|^2+\left\|\sqrt{\frac{\beta}{\mu}}(p_1-p_2)\right\|^2} \tag{4.18}$$

That is, we have established that

$$\left|\mathcal{B}_{\text{stab}}(\mathbf{W},\mathbf{U})\right| \leq 2\|\mathbf{W}\|_{\text{stab}}\|\mathbf{U}\|_{\text{stab}} \tag{4.19}$$

which completes the proof. □

THEOREM 4.3. *(Coercivity) The bilinear form is coercive. That is, the bilinear form is bounded below.*

PROOF. The coercivity of the bilinear form can be established from the definition of $\|\cdot\|_{\text{stab}}$ and Proposition 4.1 (i.e., $\|\cdot\|_{\text{stab}}$ is a norm on $\mathbb{W}$) as

$$\|\mathbf{W}\|^2_{\text{stab}} = \mathcal{B}_{\text{stab}}(\mathbf{W},\mathbf{W}) \quad \forall \mathbf{W}\in\mathbb{W} \tag{4.20}$$

□

Given the coercivity and boundedness of the bilinear form and the continuity of the linear functional, one can conclude that the proposed mixed weak formulation is well-posed by invoking the Lax-Milgram theorem [Brenner and Scott, 1994].

4.1. Convergence and error analysis of the finite element formulation. We decompose the computational domain into "$Nele$" subdomains (which will be the elements in the context of the finite element method) such that

$$\overline{\Omega} = \bigcup_{e=1}^{Nele} \overline{\Omega}^e \tag{4.21}$$

where a superposed bar indicates the set closure. We denote the finite element solution by $\mathbf{U}^h$. That is,

$$\mathbf{U}^h = (\mathbf{u}_1^h(\mathbf{x}), \mathbf{u}_2^h(\mathbf{x}), p_1^h(\mathbf{x}), p_2^h(\mathbf{x})) \tag{4.22}$$

Likewise,

$$\mathbf{W}^h = (\mathbf{w}_1^h(\mathbf{x}), \mathbf{w}_2^h(\mathbf{x}), q_1^h(\mathbf{x}), q_2^h(\mathbf{x})) \tag{4.23}$$

If we denote the set of all polynomials up to and including m-th order over a set K by $\mathscr{P}^m(K)$, and the set of all continuous functions defined on $\overline{\Omega}$ (which is the set closure of Ω) by $C^0(\overline{\Omega})$, then the following finite-dimensional spaces can be defined:

$$\mathcal{U}_1^h := \left\{\mathbf{u}_1^h(\mathbf{x})\in\mathcal{U}_1 \;\middle|\; \mathbf{u}_1^h(\mathbf{x})\in\left(C^0(\overline{\Omega})\right)^{nd}; \mathbf{u}_1^h(\mathbf{x})|_{\Omega^e}\in\left(\mathscr{P}^k(\Omega^e)\right)^{nd}; e=1,\cdots,Nele\right\} \tag{4.24a}$$

$$\mathcal{U}_2^h := \left\{\mathbf{u}_2^h(\mathbf{x})\in\mathcal{U}_2 \;\middle|\; \mathbf{u}_2^h(\mathbf{x})\in\left(C^0(\overline{\Omega})\right)^{nd}; \mathbf{u}_2^h(\mathbf{x})|_{\Omega^e}\in\left(\mathscr{P}^k(\Omega^e)\right)^{nd}; e=1,\cdots,Nele\right\} \tag{4.24b}$$

$$\mathcal{W}_1^h := \left\{\mathbf{w}_1^h(\mathbf{x})\in\mathcal{W}_1 \;\middle|\; \mathbf{w}_1^h(\mathbf{x})\in\left(C^0(\overline{\Omega})\right)^{nd}; \mathbf{w}_1^h(\mathbf{x})|_{\Omega^e}\in\left(\mathscr{P}^k(\Omega^e)\right)^{nd}; e=1,\cdots,Nele\right\} \tag{4.24c}$$

$$\mathcal{W}_2^h := \left\{\mathbf{w}_2^h(\mathbf{x})\in\mathcal{W}_2 \;\middle|\; \mathbf{w}_2^h(\mathbf{x})\in\left(C^0(\overline{\Omega})\right)^{nd}; \mathbf{w}_2^h(\mathbf{x})|_{\Omega^e}\in\left(\mathscr{P}^k(\Omega^e)\right)^{nd}; e=1,\cdots,Nele\right\} \tag{4.24d}$$

$$\mathcal{Q}^h := \left\{\left(p_1^h,p_2^h\right)\in\mathcal{Q} \;\middle|\; p_1^h(\mathbf{x}),p_2^h(\mathbf{x})\in C^0(\overline{\Omega}); p_1^h(\mathbf{x}),p_2^h(\mathbf{x})|_{\Omega^e}\in\mathscr{P}^1(\Omega^e); e=1,\cdots,Nele\right\} \tag{4.24e}$$

We define the corresponding product spaces as follows:

$$\mathbb{U}^h = \mathcal{U}_1^h \times \mathcal{U}_2^h \times \mathcal{Q}^h, \quad \text{and} \quad \mathbb{W}^h = \mathcal{W}_1^h \times \mathcal{W}_2^h \times \mathcal{Q}^h \tag{4.25}$$

It is important to note that $\mathbb{W}^h$ and $\mathbb{U}^h$ are closed linear subspaces of $\mathbb{W}$ and $\mathbb{U}$, respectively. The finite element formulation corresponding to the proposed stabilized mixed formulation reads: Find $\mathbf{U}^h \in \mathbb{U}^h$ such that we have

$$\mathcal{B}_{\text{stab}}(\mathbf{W}^h; \mathbf{U}^h) = \mathcal{L}_{\text{stab}}(\mathbf{W}^h) \quad \forall \mathbf{W}^h \in \mathbb{W}^h \tag{4.26}$$

In a given coordinate system, we denote $\mathbf{x} = (x_1, \cdots, x_{nd})$. For a given multi-index (i.e., tuple) of non-negative integers, $\alpha = (\alpha_1, \cdots, \alpha_{nd})$, with order $|\alpha| = \alpha_1 + \cdots + \alpha_{nd}$, the corresponding partial derivative of a scalar field, $p(\mathbf{x})$, can be written as follows:

$$D^\alpha p(\mathbf{x}) = \frac{\partial^{|\alpha|} p(\mathbf{x})}{\partial x_1^{\alpha_1} \partial x_2^{\alpha_2} \cdots \partial x_{nd}^{\alpha_{nd}}} \tag{4.27}$$

Using the above notation, the s^{th} Sobolev semi-norm, $|\cdot|_s$, for scalar and vector fields can be compactly written as follows:

$$|p|_s^2 = |p|_{H^s(\Omega;L)}^2 = \sum_{|\alpha|=s} \int_\Omega \left(L^s D^\alpha p(\mathbf{x})\right)^2 \mathrm{d}\Omega \tag{4.28}$$

$$|\mathbf{u}|_s^2 = |\mathbf{u}|_{H^s(\Omega;L)}^2 = \sum_{|\alpha|=s} \sum_{i=1}^{nd} \int_\Omega \left(L^s D^\alpha u_i(\mathbf{x})\right)^2 \mathrm{d}\Omega \tag{4.29}$$

where $\sum_{|\alpha|=s}$ denotes the summation over all the possible tuples of non-negative integers with order s, and L denotes the characteristic length of the domain.

REMARK 4.1. *Although the notation introduced in equation (4.27) is common in the theory of partial differential equations (e.g., [Evans, 1998]), it may not be that common in the engineering literature. For the benefit of the reader, we provide the following few examples to make the notation more apparent:*

$$\text{if } nd = 2,\ \mathbf{x} = (x_1, x_2), \alpha = (2, 1) \text{ then } |\alpha| = 3 \text{ and } D^\alpha p(\mathbf{x}) = \frac{\partial^3 p(\mathbf{x})}{\partial x_1^2 \partial x_2}$$

$$\text{if } nd = 3,\ \mathbf{x} = (x_1, x_2, x_3), \alpha = (3, 0, 6) \text{ then } |\alpha| = 9 \text{ and } D^\alpha p(\mathbf{x}) = \frac{\partial^9 p(\mathbf{x})}{\partial x_1^3 \partial x_3^6}$$

We now show the consistency of the formulation, and then establish the stability. We also obtain the rates of convergence with the mesh refinement and the order of interpolation. To this end, the error $\mathbf{E}$ is defined as

$$\mathbf{E} = \mathbf{U}^h - \mathbf{U} \tag{4.30}$$

We employ the following standard decomposition of error (e.g., see [Brenner and Scott, 1994]):

$$\mathbf{E} = \mathbf{U}^h - \mathbf{U} = \underbrace{\mathbf{U}^h - \widetilde{\mathbf{U}}^h}_{\text{approximation error}} + \underbrace{\widetilde{\mathbf{U}}^h - \mathbf{U}}_{\text{interpolation error}} = \mathbf{E}^h + \mathbf{H} \tag{4.31}$$

where $\widetilde{\mathbf{U}}^h$ denotes the interpolate of $\mathbf{U}$ onto $\mathbb{U}^h$, $\mathbf{E}^h$ is the approximation error and $\mathbf{H}$ denotes the interpolation error. The interpolation error $\mathbf{H}$ satisfies the following standard inequality [Brezzi

and Fortin, 1991]:

$$\|\mathbf{H}\|_{\text{stab}} \leq C_1 \left(\frac{h}{L}\right)^{k+1} |\mathbf{u}_1|_{k+1} + C_2 \left(\frac{h}{L}\right)^{l+1} |\mathbf{u}_2|_{l+1} + C_3 \left(\frac{h}{L}\right)^{m} |p_1|_{m+1} + C_4 \left(\frac{h}{L}\right)^{n} |p_2|_{n+1} \tag{4.32}$$

In the above inequality, h is the characteristic mesh parameter, L is a characteristic dimension of the domain Ω, and k, l, m, and n are natural numbers. As mentioned earlier, we have taken h to be the maximum edge length in the mesh. However, the results presented herein are equally valid for other choices of h; for example, the maximum element diameter. The constants C_1, C_2, C_3 and C_4 are defined as follows:

$$\begin{aligned} C_1 &= C_0 \sup_{\mathbf{x}\in\Omega} \left(\mu(\mathbf{x}) k_1^{-1}(\mathbf{x})\right)^{\frac{1}{2}}, \quad C_2 = C_0 \sup_{\mathbf{x}\in\Omega} \left(\mu(\mathbf{x}) k_2^{-1}(\mathbf{x})\right)^{\frac{1}{2}}, \\ C_3 &= \frac{C_0}{L} \sup_{\mathbf{x}\in\Omega} \left(\frac{1}{\mu(\mathbf{x})} k_1(\mathbf{x})\right)^{\frac{1}{2}} \quad \text{and} \quad C_4 = \frac{C_0}{L} \sup_{\mathbf{x}\in\Omega} \left(\frac{1}{\mu(\mathbf{x})} k_2(\mathbf{x})\right)^{\frac{1}{2}} \end{aligned} \tag{4.33}$$

where C_0 is a non-dimensional constant. Note that C_1, C_2, C_3 and C_4 are independent of h, $\mathbf{u}_1$, $\mathbf{u}_2$, p_1 and p_2.

THEOREM 4.4. *(Consistency) The error in the finite element solution satisfies*

$$\mathcal{B}_{\text{stab}}(\mathbf{W}^h; \mathbf{E}) = 0 \quad \forall \mathbf{W}^h \in \mathbb{W}^h \subset \mathbb{W} \tag{4.34}$$

PROOF. The finite element solution satisfies

$$\mathcal{B}_{\text{stab}}(\mathbf{W}^h, \mathbf{U}^h) = \mathcal{L}_{\text{stab}}(\mathbf{W}^h) \quad \forall \mathbf{W}^h \in \mathbb{W}^h \tag{4.35}$$

The exact solution clearly satisfies

$$\mathcal{B}_{\text{stab}}(\mathbf{W}^h, \mathbf{U}) = \mathcal{L}_{\text{stab}}(\mathbf{W}^h) \quad \forall \mathbf{W}^h \in \mathbb{W}^h \tag{4.36}$$

By subtracting the above two equations and using the linearity of the bilinear form $\mathcal{B}_{\text{stab}}(\cdot,\cdot)$ in the second slot, we obtain the desired result. □

THEOREM 4.5. *(Convergence) For all $\tilde{\mathbf{U}}^h \in \mathbb{U}^h$, the error satisfies*

$$\|\mathbf{E}\|_{\text{stab}} \leq C \|\mathbf{H}\|_{\text{stab}} \tag{4.37}$$

where C is a non-dimensional constant.

PROOF. Noting the decomposition of error mentioned in equation (4.31) (i.e., $\mathbf{E} = \mathbf{E}^h + \mathbf{H}$), we proceed as follows:

$$\begin{aligned} \|\mathbf{E}\|^2_{\text{stab}} &= \mathcal{B}_{\text{stab}}(\mathbf{E}; \mathbf{E}) && \text{(definition of } \|\cdot\|_{\text{stab}} \text{ norm)} \\ &= \mathcal{B}_{\text{stab}}(\mathbf{E}^h + \mathbf{H}; \mathbf{E}) && \text{(standard decomposition of } \mathbf{E}) \\ &= \mathcal{B}_{\text{stab}}(\mathbf{E}^h; \mathbf{E}) + \mathcal{B}_{\text{stab}}(\mathbf{H}; \mathbf{E}) && \text{(bilinearity)} \\ &= \mathcal{B}_{\text{stab}}(\mathbf{H}; \mathbf{E}) && \text{(consistency)} \end{aligned} \tag{4.38}$$

We now estimate $\mathcal{B}_{\text{stab}}(\mathbf{H}; \mathbf{E})$. To this end, we denote the components of $\mathbf{E}$ and $\mathbf{H}$ as follows:

$$\mathbf{E} = \{\mathbf{e}_{\mathbf{u}_1}, \mathbf{e}_{\mathbf{u}_2}, e_{p_1}, e_{p_2}\}, \quad \text{and} \quad \mathbf{H} = \{\boldsymbol{\eta}_{\mathbf{u}_1}, \boldsymbol{\eta}_{\mathbf{u}_2}, \eta_{p_1}, \eta_{p_2}\}$$

By repeated use of Cauchy-Schwartz and Peter-Paul inequalities [Hunter and Nachtergaele, 2001], we estimate $\mathcal{B}_{\text{stab}}(\mathbf{H}; \mathbf{E})$ as follows:

$$\mathcal{B}_{\text{stab}}(\mathbf{H}; \mathbf{E}) = \mathcal{B}_{\text{stab}}(\boldsymbol{\eta}_{\mathbf{u}_1}, \boldsymbol{\eta}_{\mathbf{u}_2}, \eta_{p_1}, \eta_{p_2}; \mathbf{e}_{\mathbf{u}_1}, \mathbf{e}_{\mathbf{u}_2}, e_{p_1}, e_{p_2})$$

$$
\begin{aligned}
&= (\boldsymbol{\eta}_{\mathbf{u}_1}; \mu\mathbf{K}_1^{-1}\mathbf{e}_{\mathbf{u}_1}) - (\mathrm{div}[\boldsymbol{\eta}_{\mathbf{u}_1}]; e_{p_1}) + (\eta_{p_1}; \mathrm{div}[\mathbf{e}_{\mathbf{u}_1}]) \\
&+ (\boldsymbol{\eta}_{\mathbf{u}_2}; \mu\mathbf{K}_2^{-1}\mathbf{e}_{\mathbf{u}_2}) - (\mathrm{div}[\boldsymbol{\eta}_{\mathbf{u}_2}]; e_{p_2}) + (\eta_{p_2}; \mathrm{div}[\mathbf{e}_{\mathbf{u}_2}]) \\
&- \frac{1}{2}\left(\boldsymbol{\eta}_{\mathbf{u}_1}; \mu\mathbf{K}_1^{-1}\mathbf{e}_{\mathbf{u}_1}\right) - \frac{1}{2}\left(\boldsymbol{\eta}_{\mathbf{u}_1}; \mathrm{grad}[e_{p_1}]\right) + \frac{1}{2}\left(\mathrm{grad}[\eta_{p_1}]; \mathbf{e}_{\mathbf{u}_1}\right) + \frac{1}{2}\left(\mathrm{grad}[\eta_{p_1}]; \frac{1}{\mu}\mathbf{K}_1\mathrm{grad}[e_{p_1}]\right) \\
&- \frac{1}{2}\left(\boldsymbol{\eta}_{\mathbf{u}_2}; \mu\mathbf{K}_2^{-1}\mathbf{e}_{\mathbf{u}_2}\right) - \frac{1}{2}\left(\boldsymbol{\eta}_{\mathbf{u}_2}; \mathrm{grad}[e_{p_2}]\right) + \frac{1}{2}\left(\mathrm{grad}[\eta_{p_2}]; \mathbf{e}_{\mathbf{u}_2}\right) + \frac{1}{2}\left(\mathrm{grad}[\eta_{p_2}]; \frac{1}{\mu}\mathbf{K}_2\mathrm{grad}[e_{p_2}]\right) \\
&+ ((\eta_{p_1} - \eta_{p_2}); \beta/\mu(e_{p_1} - e_{p_2})) \\
&\leq \frac{1}{2}\left\{\varepsilon_1\|\sqrt{\mu}\mathbf{K}_1^{-1/2}\boldsymbol{\eta}_{\mathbf{u}_1}\|^2 + \frac{1}{\varepsilon_1}\|\sqrt{\mu}\mathbf{K}_1^{-1/2}\mathbf{e}_{\mathbf{u}_1}\|^2 + \varepsilon_2\|\sqrt{\mu}\mathbf{K}_1^{-1/2}\boldsymbol{\eta}_{\mathbf{u}_1}\|^2\right. \\
&\quad + \frac{1}{\varepsilon_2}\|\frac{1}{\sqrt{\mu}}\mathbf{K}_1^{1/2}\mathrm{grad}[e_{p_1}]\|^2 + \varepsilon_3\|\frac{1}{\sqrt{\mu}}\mathbf{K}_1^{1/2}\mathrm{grad}[\eta_{p_1}]\|^2 + \frac{1}{\varepsilon_3}\|\sqrt{\mu}\mathbf{K}_1^{-1/2}\mathbf{e}_{\mathbf{u}_1}\|^2 \\
&\quad + \varepsilon_4\|\sqrt{\mu}\mathbf{K}_2^{-1/2}\boldsymbol{\eta}_{\mathbf{u}_2}\|^2 + \frac{1}{\varepsilon_4}\|\sqrt{\mu}\mathbf{K}_2^{-1/2}\mathbf{e}_{\mathbf{u}_2}\|^2 + \varepsilon_5\|\sqrt{\mu}\mathbf{K}_2^{-1/2}\boldsymbol{\eta}_{\mathbf{u}_2}\|^2 \\
&\quad + \frac{1}{\varepsilon_5}\|\frac{1}{\sqrt{\mu}}\mathbf{K}_2^{1/2}\mathrm{grad}[e_{p_2}]\|^2 + \varepsilon_6\|\frac{1}{\sqrt{\mu}}\mathbf{K}_2^{1/2}\mathrm{grad}[\eta_{p_2}]\|^2 + \frac{1}{\varepsilon_6}\|\sqrt{\mu}\mathbf{K}_2^{-1/2}\mathbf{e}_{\mathbf{u}_2}\|^2 \\
&\quad + \frac{\varepsilon_7}{2}\|\sqrt{\mu}\mathbf{K}_1^{-1/2}\boldsymbol{\eta}_{\mathbf{u}_1}\|^2 + \frac{1}{2\varepsilon_7}\|\sqrt{\mu}\mathbf{K}_1^{-1/2}\mathbf{e}_{\mathbf{u}_1}\|^2 + \frac{\varepsilon_8}{2}\|\sqrt{\mu}\mathbf{K}_1^{-1/2}\boldsymbol{\eta}_{\mathbf{u}_1}\|^2 \\
&\quad + \frac{1}{2\varepsilon_8}\|\frac{1}{\sqrt{\mu}}\mathbf{K}_1^{1/2}\mathrm{grad}[e_{p_1}]\|^2 + \frac{\varepsilon_9}{2}\|\frac{1}{\sqrt{\mu}}\mathbf{K}_1^{1/2}\mathrm{grad}[\eta_{p_1}]\|^2 + \frac{1}{2\varepsilon_9}\|\sqrt{\mu}\mathbf{K}_1^{-1/2}\mathbf{e}_{\mathbf{u}_1}\|^2 \\
&\quad + \frac{\varepsilon_{10}}{2}\|\frac{1}{\sqrt{\mu}}\mathbf{K}_1^{1/2}\mathrm{grad}[\eta_{p_1}]\|^2 + \frac{1}{2\varepsilon_{10}}\|\frac{1}{\sqrt{\mu}}\mathbf{K}_1^{1/2}\mathrm{grad}[e_{p_1}]\|^2 + \frac{\varepsilon_{11}}{2}\|\sqrt{\mu}\mathbf{K}_2^{-1/2}\boldsymbol{\eta}_{\mathbf{u}_2}\|^2 \\
&\quad + \frac{1}{2\varepsilon_{11}}\|\sqrt{\mu}\mathbf{K}_2^{-1/2}\mathbf{e}_{\mathbf{u}_2}\|^2 + \frac{\varepsilon_{12}}{2}\|\sqrt{\mu}\mathbf{K}_2^{-1/2}\boldsymbol{\eta}_{\mathbf{u}_2}\|^2 + \frac{1}{2\varepsilon_{12}}\|\frac{1}{\sqrt{\mu}}\mathbf{K}_2^{1/2}\mathrm{grad}[e_{p_2}]\|^2 \\
&\quad + \frac{\varepsilon_{13}}{2}\|\frac{1}{\sqrt{\mu}}\mathbf{K}_2^{1/2}\mathrm{grad}[\eta_{p_2}]\|^2 + \frac{1}{2\varepsilon_{13}}\|\sqrt{\mu}\mathbf{K}_2^{-1/2}\mathbf{e}_{\mathbf{u}_2}\|^2 + \frac{\varepsilon_{14}}{2}\|\frac{1}{\sqrt{\mu}}\mathbf{K}_2^{1/2}\mathrm{grad}[\eta_{p_2}]\|^2 \\
&\quad + \frac{1}{2\varepsilon_{14}}\|\frac{1}{\sqrt{\mu}}\mathbf{K}_2^{1/2}\mathrm{grad}[e_{p_2}]\|^2 + \varepsilon_{15}\|\left(\beta/\mu\right)^{1/2}(\eta_{p_1} - \eta_{p_2})\|^2 \\
&\quad \left. + \frac{1}{\varepsilon_{15}}\|\left(\beta/\mu\right)^{1/2}(e_{p_1} - e_{p_2})\|^2\right\}
\end{aligned} \tag{4.39}
$$

where $\varepsilon_i,\ i = 1, \ldots, 15$ are positive constants. By choosing

$$
\begin{aligned}
2\varepsilon_1 = 2\varepsilon_3 = 2\varepsilon_4 = 2\varepsilon_6 = \varepsilon_7 = \varepsilon_9 = \varepsilon_{11} = \varepsilon_{13} = 10 \quad \text{and} \\
2\varepsilon_2 = 2\varepsilon_5 = \varepsilon_8 = \varepsilon_{10} = \varepsilon_{12} = \varepsilon_{14} = 6,\ \varepsilon_{15} = 1
\end{aligned} \tag{4.40}
$$

we obtain the following inequality:

$$
\begin{aligned}
\mathcal{B}_{\mathrm{stab}}(\mathbf{H}; \mathbf{E}) &\leq \frac{1}{2}\left\{\|\mathbf{E}\|_{\mathrm{stab}}^2 + 16\|\sqrt{\mu}\mathbf{K}_1^{-1/2}\boldsymbol{\eta}_{\mathbf{u}_1}\|^2 + 13\|\frac{1}{\sqrt{\mu}}\mathbf{K}_1^{1/2}\mathrm{grad}[\eta_{p_1}]\|^2\right. \\
&\qquad \left. + 16\|\sqrt{\mu}\mathbf{K}_2^{-1/2}\boldsymbol{\eta}_{\mathbf{u}_2}\|^2 + 13\|\frac{1}{\sqrt{\mu}}\mathbf{K}_2^{1/2}\mathrm{grad}[\eta_{p_2}]\|^2 + \|\left(\beta/\mu\right)^{1/2}(\eta_{p_1} - \eta_{p_2})\|^2\right\} \\
&\leq \frac{1}{2}\|\mathbf{E}\|_{\mathrm{stab}}^2 + 16\|\mathbf{H}\|_{\mathrm{stab}}^2
\end{aligned} \tag{4.41}
$$

Noting equation (4.38) we have

$$
\mathcal{B}_{\mathrm{stab}}(\mathbf{H}; \mathbf{E}) = \|\mathbf{E}\|_{\mathrm{stab}}^2 \leq 32\|\mathbf{H}\|_{\mathrm{stab}}^2 \tag{4.42}
$$

which gives the following estimate of the total error in terms of the interpolation error:

$$\|\mathbf{E}\|_{\text{stab}} \leq 4\sqrt{2}\|\mathbf{H}\|_{\text{stab}} \tag{4.43}$$

This completes the proof. □

The set of choices made for constants, ε_i $(i = 1, \cdots, 15)$, is one of many such ones to obtain an upper bound for $\mathcal{B}_{\text{stab}}(\mathbf{H}; \mathbf{E})$ in terms of the total error, $\mathbf{E}$, and the interpolation error, $\mathbf{H}$. We do not claim that this selection of constants is optimal. Certainly, the estimate (4.41) and the subsequent ones are not sharp. Although obtaining sharp estimates is of theoretical significance in mathematical analysis, it is not crucial to establish the convergence of the proposed stabilized formulation. We, therefore, do not pursue further with respect to obtaining the optimal choices for the constants ε_i, and for obtaining a sharp estimate for $\mathcal{B}_{\text{stab}}(\mathbf{H}; \mathbf{E})$.

5. PATCH TESTS AND NUMERICAL CONVERGENCE ANALYSIS

In order to assess the convergence behavior of a numerical (finite element) formulation and to determine whether it is programmed correctly, patch tests are commonly used. In this section, we first illustrate the performance of the proposed stabilized mixed formulation under the equal-order interpolation for all the field variables using one-dimensional and three-dimensional constant-flow patch tests. We also compare the results obtained under the proposed stabilized mixed formulation with that of the classical mixed formulation (which is based on the Galerkin formalism). We then perform a systematic numerical convergence analysis of the proposed stabilized mixed formulation under h- and p-refinements, and compare the obtained rates of convergence with the theory.

Under our studies on patch tests and numerical convergence analysis, we often use the term machine precision, which is the smallest difference between two numbers that the computing machine recognizes [Heath, 2001]. Mathematically, the machine precision of a computing machine, ϵ_{mach}, satisfies

$$\begin{aligned} (1+\epsilon) - 1 = 0 \qquad & \forall \epsilon < \epsilon_{\text{mach}} \\ \text{and } (1+\epsilon) - 1 = \epsilon \neq 0 \quad & \forall \epsilon > \epsilon_{\text{mach}} \end{aligned}$$

It is important to note that the machine precision depends on the underlying hardware of the computer, and hence, its value can vary from one computer to another. It is also important to note that the machine precision of a computer is not the smallest number that the computer can represent. To put the things quantitatively, the machine precision on a 32-bit machine is approximately 10^{-7} and on a 64-bit machine, it is approximately 10^{-16} [Higham, 2002]. On the other hand, the smallest positive numbers that a 32-bit machine and a 64-bit machine can represent are approximately 10^{-38} and 10^{-308}, respectively [Higham, 2002].

5.1. One-dimensional constant flow patch test. The purpose of solving the one-dimensional example is to provide a simple numerical tool for testing whether the proposed mixed formulation satisfies the LBB condition. Figure 1(a) provides a pictorial description of the problem, and Table 1 provides the data-set for this problem. The domain is a line of unit length along x direction. On the left end of the domain, pressures p_1^{L} and p_2^{L} are prescribed in macro- and micro-pore networks, respectively. Similarly, on the right end of the domain, p_1^{R} and p_2^{R} are, respectively, prescribed in the macro- and the micro-pore networks. Since a pressure boundary condition is prescribed for at least one of the pore-networks, the condition of vanishing mean pressure in one of pore-networks in

the function space $\mathcal{Q}$ (which is defined in equation (3.2f)) is not appropriate for this problem. See the discussion in Section 3.

TABLE 1. Data-set for one-dimensional constant flow patch test and 1D numerical convergence analysis.

Parameter	Value
γb	0.0
L	1.0
μ	1.0
β	1.0
k_1	1.0
k_2	0.01
p_1^L	10.0
p_1^R	1.0
p_2^L	10.0
p_2^R	1.0

The governing equations can be written as follows:

$$\mu k_1^{-1}\mathbf{u}_1(\mathbf{x}) + \frac{dp_1}{dx} = 0 \qquad \text{in } (0, L) \tag{5.1a}$$

$$\mu k_2^{-1}\mathbf{u}_2(\mathbf{x}) + \frac{dp_1}{dx} = 0 \qquad \text{in } (0, L) \tag{5.1b}$$

$$\frac{du_1}{dx} = +\chi(x) \qquad \text{in } (0, L) \tag{5.1c}$$

$$\frac{du_2}{dx} = -\chi(x) \qquad \text{in } (0, L) \tag{5.1d}$$

$$p_1(x = 0) = p_1^{\mathrm{L}}, \quad p_1(x = L) = p_1^{\mathrm{R}} \tag{5.1e}$$

$$p_2(x = 0) = p_2^{\mathrm{L}}, \quad p_2(x = L) = p_2^{\mathrm{R}} \tag{5.1f}$$

It should be noted that the quantities used in equations (5.1a)–(5.1f) are non-dimensional. More details on non-dimensionalization procedure can be found in [Nakshatrala et al., 2016]. In this boundary value problem, k_1 and k_2 are assumed to be independent of x and the mass transfer between the two pore-networks takes the following form:

$$\chi(x) = -\left(p_1(x) - p_2(x)\right) \tag{5.2}$$

The analytical solution for this simple 1D problem includes constant velocities and linearly varying pressures (from p_i^L to p_i^R) at each pore-network along the x direction.

Figure 2 shows the numerical results for pressure and velocity profiles in the two pore-networks under Galerkin and the proposed stabilized mixed formulations. The values of velocity vector fields in the two pore-networks match the analytical solutions under both proposed the stabilized mixed formulation and the Galerkin formulation. As can be seen in Figures 2(c) and 2(d), under the stabilized mixed formulation, pressures in the two pore-networks vary linearly from the prescribed value at the left end ($p_i^{\mathrm{L}},\ i = 1, 2$) to the prescribed one at the right end ($p_i^{\mathrm{R}},\ i = 1, 2$). These results are in agreement with the corresponding analytical solutions up to the machine precision, thus showing that the proposed formulation performs well and that it satisfies the 1D patch test.

However, under the Galerkin formulation, spurious oscillations are observed in the pressure fields in both macro- and micro-networks even for equal-order interpolation.

5.2. Three-dimensional constant flow patch test. Previous research studies have shown that many existing numerical formulations cannot perform well when they are extended to 3D settings [Hughes et al., 2006; Nakshatrala et al., 2006]. Herein, using the 3D constant flow patch test we will show that the proposed stabilized mixed formulation performs well even in 3D settings and it's capable of satisfying the LBB condition. To illustrate this, we consider the unit cube computational domain shown in Figure 1(b). On the left and right faces, pressures $p_i^{\mathrm{L}},\ i = 1, 2$ and $p_i^{\mathrm{R}},\ i = 1, 2$ are prescribed respectively where $i = 1$ denotes the macro-pore network and $i = 2$ represents the micro-pore network. On the other faces, the velocity boundary condition is prescribed in the two pore-networks (i.e., $\mathbf{u}_i \cdot \widehat{\mathbf{n}} = 0,\ i = 1, 2$). Table 2 provides the parameter values for this test problem.

TABLE 2. Data-set for three-dimensional constant flow patch test.

Parameter	Value
$\gamma\mathbf{b}$	$\{0.0, 0.0, 0.0\}$
L_x	1.0
L_y	1.0
μ	1.0
β	1.0
k_1	1.0
k_2	0.01
p_1^L	10.0
p_1^R	1.0
p_2^L	10.0
p_2^R	1.0

The analytical solution pair for this constant flow patch test includes constant velocity along x direction and pressure linearly varying along x direction at each pore-network. Figure 3 shows the numerical results for pressure profiles associated with the two pore-networks under Galerkin and the stabilized mixed formulations. It is observed that the Galerkin formulation produces spurious oscillations in micro- and macro-pressures even for equal-order interpolation. This indicates that Galerkin formulation cannot accurately predict pressure variations and that the results are not stable. These oscillations are completely eliminated by the proposed stabilized mixed formulation, thus illustrating the stability of the solution. This verifies that the proposed numerical formulation performs well and satisfies the 3D constant flow patch test.

5.3. Numerical convergence under h- and p-refinements. In this subsection, the convergence behavior of the proposed stabilized mixed formulation is evaluated. For this purpose, the convergence analysis is performed in 1D and 2D settings. The convergence rates are obtained under two different approaches. The first method is called *h-refinement* where the number of elements is increased and hence the size of elements (denoted by "h") in the domain is decreased. The convergence rates under h-refinement are obtained for various polynomial orders. In the second approach, the so-called *p-refinement*, the convergence rate is calculated by changing the order of polynomial while the total number of elements in the domain is kept fixed (nx = 5).

5.3.1. *1D numerical convergence analysis.* For the convergence analysis in the 1D setting, we select the previously defined one-dimensional patch test (subsection 5.1). In Figures 4 and 5, the convergence rates under h- and p-refinements are shown for the L_2-norm of the velocity fields in the macro- and micro-pore networks (denoted by "L_2 u_1" and "L_2 u_2", respectively), the L_2-norm of the pressure fields in the macro- and micro-pore networks (denoted by "L_2 p_1" and "L_1 p_2", respectively), and the H^1-norm of the pressure fields in the macro- and micro-pore networks (denoted by "H^1 p_1" and "H^1 p_2", respectively). As can be seen in these figures, the rate of convergence for h-refinement is polynomial and for p-refinement is exponential, which are in accordance with the theory.

5.3.2. *2D numerical convergence analysis.* The convergence analysis in the 2D setting is performed on the unit square domain shown in Figure 6. The macro- and micro-pressures are prescribed on the four sides of the computational domain. Table 3 provides the parameter values for the 2D convergence analysis. For convenience, let us define

TABLE 3. Data-set for 2D numerical convergence analysis.

Parameter	Value
$\gamma\mathbf{b}$	$\{0.0, 0.0\}$
L_x	1.0
L_y	1.0
μ	1.0
β	1.0
k_1	1.0
k_2	0.1
η	$\sqrt{11} \simeq 3.3166$
$p_i^{\text{left}},\ i=1,2$	Obtained by evaluating
$p_i^{\text{right}},\ i=1,2$	the analytical solution
$p_i^{\text{top}},\ i=1,2$	(equations (5.6) and (5.7))
$p_i^{\text{bottom}},\ i=1,2$	on the respective boundaries.

$$\eta := \sqrt{\beta \frac{k_1 + k_2}{k_1 k_2}} \tag{5.3}$$

Then the analytical solution for the velocity fields can be defined as

$$\mathbf{u}_1(x,y) = -k_1 \begin{pmatrix} \exp(\pi x)\sin(\pi y) \\ \exp(\pi x)\cos(\pi y) \end{pmatrix} + \begin{pmatrix} 0 \\ \frac{\eta}{\beta}\exp(\eta y) \end{pmatrix} \tag{5.4}$$

$$\mathbf{u}_2(x,y) = -k_2 \begin{pmatrix} \exp(\pi x)\sin(\pi y) \\ \exp(\pi x)\cos(\pi y) \end{pmatrix} - \begin{pmatrix} 0 \\ \frac{\eta}{\beta}\exp(\eta y) \end{pmatrix} \tag{5.5}$$

The analytical solution for the pressure fields can then be obtained as follows:

$$p_1(x,y) = \frac{\mu}{\pi}\exp(\pi x)\sin(\pi y) - \frac{\mu}{\beta k_1}\exp(\eta y) \tag{5.6}$$

$$p_2(x,y) = \frac{\mu}{\pi}\exp(\pi x)\sin(\pi y) + \frac{\mu}{\beta k_2}\exp(\eta y) \tag{5.7}$$

Figure 7 provides the convergence rates under h-refinement for the L_2-norm and the H^1-norm of the pressure fields in the macro- and micro-pore networks. The results under p-refinement for

the L_2-norm of the pressure fields are also provided in Figure 8. The rates of convergence for h- and p-refinements are respectively polynomial and exponential, which are in accordance with the theory. As can be seen, the error under p-refinement flattened out around 10^{-16} for larger number of degrees-of-freedom. This is expected as the machine precision on a 64-bit machine is around 10^{-16}. The results obtained from the one-dimensional and two-dimensional problems verify that the proposed stabilized mixed formulation is convergent.

6. REPRESENTATIVE NUMERICAL RESULTS

In the previous section, the convergence behavior of the proposed mixed formulation has been assessed using patch tests and numerical convergence analysis. In this section, using representative problems with relevance to technological applications, the flow characteristics in the porous media exhibiting double porosity/permeability are studied. The performance of the Nitsche's method is illustrated using two-dimensional candle filter problem and three-dimensional hollow sphere problem.

6.1. Two-dimensional candle filter problem. The aim of this problem is to show how the velocity boundary conditions can be enforced weakly in two-dimensional settings using Nitsche's method. This two-dimensional boundary value problem is a model of water flow in candle filters which are commonly used for purifying drinking water. The domain consists of a circular disc of inner radius of $r_i = a$ and outer radius of $r_o = 1$. For the macro-pore network, the inner surface is subjected to a pressure ($p_1(r = r_i) = 1.0$ atm), and the outer surface is exposed to the atmosphere ($p_1(r = r_o) = 0$). For the micro-pore network, no discharge is allowed from the inner and outer surfaces (i.e. $\mathbf{u}_2 \cdot \widehat{\mathbf{n}} = 0$). Figure 9 shows the computational domain for this problem as well as the boundary conditions. Considering the underlying symmetry in the problem, the velocities and pressures in the two pore-networks are assumed to be functions of r only. Parameter values for this test problem are provided in Table 4.

TABLE 4. Data-set for two-dimensional candle filter problem.

Parameter	Value
$\gamma\mathbf{b}$	$\{0.0, 0.0\}$
r_o	1.0
r_i	0.3
μ	1.0
β	1.0
k_1	1.0
k_2	0.01
$p_1(r = 0.3)$	1.0
$p_1(r = 1.0)$	0.0
$u_{n2}(r = 0.3)$	0.0
$u_{n2}(r = 1.0)$	0.0

The relevant governing equations in the polar coordinates can be summarized as follows:

$$\frac{\mu}{k_1}u_1 + \frac{dp_1}{dr} = 0, \quad \frac{1}{r}\frac{d(ru_1)}{dr} + (p_1 - p_2) = 0, \quad \forall r \in (a, 1) \tag{6.1a}$$

$$\frac{\mu}{k_2}u_2 + \frac{dp_2}{dr} = 0, \quad \frac{1}{r}\frac{d(ru_2)}{dr} - (p_1 - p_2) = 0, \quad \forall r \in (a, 1) \tag{6.1b}$$

$$p_1(r = a) = 1, \quad p_1(r = 1) = 0, \quad u_2(r = a) = 0, \quad u_2(r = 1) = 0 \tag{6.1c}$$

Figures 10(a) and 10(b) show the pressure and velocity profiles under the extended framework for weak enforcement of velocity boundary conditions. The micro-velocity profile implies that although there is no discharge from the micro-pore network on the boundary, there is discharge in the micro-pore network within the domain. It can be concluded that the surface pore-structure is not the only factor that characterizes the flow throughout the domain and that the internal pore-structure plays a significant role.

6.2. Three-dimensional hollow sphere problem. The hollow sphere problem is used to examine the weak enforcement of the velocity boundary conditions in 3D settings using Nitsche's method. The computational domain consists of a sphere of radius $r_o = 1.0$, at the center of which is a spherical hole of radius $r_i = a$. At the inner surface of the hole, the macro-pore network is subjected to a pressure $p_1(r = r_i) = 1$, and at the outer surface of the sphere, the macro-pore network is subjected to a pressure $p_1(r = r_o) = 0$. For the micro-pore network, there is no discharge from the inner and outer surfaces (i.e., $\mathbf{u}_2 \cdot \widehat{\mathbf{n}} = 0$). Table 5 provides the parameter values for this problem.

TABLE 5. Data-set for three-dimensional hollow sphere problem.

Parameter	Value
$\gamma\mathbf{b}$	$\{0.0, 0.0, 0.0\}$
r_o	1.0
r_i	0.3
μ	1.0
β	1.0
k_1	1.0
k_2	0.01
$p_1(r = 0.3)$	1.0
$p_1(r = 1.0)$	0.0
$u_{n2}(r = 0.3)$	0.0
$u_{n2}(r = 1.0)$	0.0

Similar to the candle filter problem, all the variables can be considered to be functions of r only due to the symmetry. Therefore, the governing equations can be written as follows:

$$\frac{\mu}{k_1}u_1 + \frac{dp_1}{dr} = 0, \quad \frac{1}{r^2}\frac{d(r^2u_1)}{dr} = -(p_1 - p_2), \quad \forall r \in (a, 1) \tag{6.2a}$$

$$\frac{\mu}{k_2}u_2 + \frac{dp_2}{dr} = 0, \quad \frac{1}{r^2}\frac{d(r^2u_2)}{dr} = +(p_1 - p_2), \quad \forall r \in (a, 1) \tag{6.2b}$$

$$p_1(r = a) = 1, \quad p_1(r = 1) = 0, \quad u_2(r = a) = 0, \quad u_2(r = 1) = 0 \tag{6.2c}$$

The numerical results for the pressures and velocity fields are shown in Figures 11(a) and 11(b). It is seen that under the extended framework for weak enforcement of velocity boundary conditions, the results are stable and although no discharge is considered for the micro-pore network on the boundary, there is discharge in the micro-pore network within the domain. The important role

of the internal pore-structure in such complex porous domains pitches a case for using advanced characterization tools like X-ray micro-computed tomography (i.e., μ-CT) [Stock, 2008].

It should be noted that in order to provide a proper visualization of the velocity fields within the domain, it has been clipped and put in a perspective view. Since an unstructured mesh has been used for this 3D domain, the visualization software (i.e., ParaView) cuts through the elements and interpolates the values to draw the contours. This introduces some dependence on the angular coordinates (see Figure 11(b)). But one does not find this angular dependence in the raw data for various angles for a given radius.

7. MECHANICS-BASED ASSESSMENT OF NUMERICAL ACCURACY

For all the problems presented in the previous sections (including the ones under the numerical convergence analysis), analytical solutions are known. For such problems, the accuracy of numerical solutions can be easily quantified by comparing them with the analytical solutions (either point-wise or in some appropriate norm). But for practical problems, analytical solutions are seldom known. The question then will be how to assess the accuracy of numerical solutions for those problems with no available analytical solution. The source of possible error in the numerical solutions could be either due to the formulation itself or in the computer implementation. Even if the formulation is known to be a converging scheme, there could be errors in the computer implementation or in setting up the problem to obtain the numerical solutions (e.g., wrong input data).

Fortunately, the solutions under the double porosity/permeability model enjoy several important mathematical properties, which can serve as *a posteriori* error measures. More importantly, these mathematical properties have strong mechanics underpinning and can be applied to any problem; in particular, they are effective for those problems without known analytical solutions. Thus, it is appropriate to refer to such an approach as *mechanics-based solution verification method*. Such a study has been undertaken for Darcy and Darcy-Brinkman equations by [Shabouei and Nakshatrala, 2016]. Herein, we extend the approach to the double porosity/permeability model and illustrate its utility and performance to assess the accuracy of numerical solutions under the proposed stabilized mixed formulation. However, it needs to be emphasized that the mechanics-based solution verification method can be applied to any numerical formulation (which necessarily need not be based on the finite element method) and to any problem.

Recently, [Nakshatrala et al., 2016] have shown that the exact solutions under the double porosity/permeability satisfy minimum dissipation theorem, Betti-type reciprocal relations and minimum total power theorem. A numerical solution need not satisfy these mathematical properties, but the associated errors can be quantified, which can serve as measures to assess the accuracy of numerical solutions. We now utilize the minimum dissipation theorem and the reciprocal relation to illustrate the approach to assess the accuracy.

7.1. *A posteriori* criterion based on the minimum dissipation theorem. Under the double porosity/permeability model, the dissipation functional takes the following form [Nakshatrala et al., 2016]:

$$\mathbf{\Phi}\left[\mathbf{u}_1, \mathbf{u}_2\right] := \sum_{i=1}^{2} \left(\int_\Omega \mu \mathbf{K}_i^{-1} \mathbf{u}_i \cdot \mathbf{u}_i \mathrm{d}\Omega + \frac{1}{2} \int_\Omega \frac{\mu}{\beta} \mathrm{div}\left[\mathbf{u}_i\right] \mathrm{div}\left[\mathbf{u}_i\right] \mathrm{d}\Omega \right) \tag{7.1}$$

Under the minimum dissipation theorem, it is assumed that $\gamma \mathbf{b}(\mathbf{x})$ is a conservative vector field and the velocity boundary conditions are prescribed on the entire boundary for both pore-networks

(i.e., $\partial\Omega = \Gamma_1^u = \Gamma_2^u$). Moreover, a pair of vector fields $(\widetilde{\mathbf{u}}_1, \widetilde{\mathbf{u}}_2)$ will be referred to as kinematically admissible if it satisfies the prescribed velocity boundary conditions and the following condition:

$$\operatorname{div}[\widetilde{\mathbf{u}}_1] + \operatorname{div}[\widetilde{\mathbf{u}}_2] = 0 \quad \text{in } \Omega \tag{7.2}$$

Of course, the pair of velocity fields under the exact solution is kinematically admissible. The minimum dissipation theorem states that the pair of velocity fields under the exact solution achieves the minimum dissipation among the set of all kinematically admissible vector fields [Nakshatrala et al., 2016].

Before we discuss how the minimum dissipation theorem can be utilized as *a posteriori* criterion, it is important to highlight the following three points regarding the relation between numerical solutions and this theorem:

(i) A numerical solution need not be the minimizer of dissipation functional. That is, in the strict sense, a numerical solution does not satisfy the minimum dissipation theorem.

(ii) More importantly, the pair of velocity fields under a numerical solution may not even be kinematically admissible.

(iii) It is not computationally attractive to find a numerical solution by solving the constrained optimization problem that results from the minimum dissipation theorem, as such a solution procedure will be very expensive; especially, for large-scale practical problems.

A description of the proposed *a posteriori* criterion based on the minimum dissipation theorem is as follows: Solve the given boundary value problem under h- or p-refinements. For each case of refinement, evaluate the total dissipation (7.1) using the obtained numerical solution. Plot the values of the dissipation with respect to characteristic mesh size h for the case of h-refinement or degrees-of-freedom in the case of p-refinement. The values of the total dissipation under the obtained numerical solutions should decrease monotonically and reach a plateau upon refinements. We provide numerical results towards the end of this section which support this trend.

A plausible reasoning for the aforesaid trend can be constructed as follows: Although the pair of velocity fields under a converging numerical formulation does not *strictly* satisfy the condition (7.2), the error in meeting this condition will be small upon adequate h- or p-refinement. Assuming that the velocity boundary conditions are accurately implemented, the minimum dissipation theorem implies that the obtained total dissipation under the numerical solution should be higher than the corresponding value under the exact solution. Moreover, for a converging formulation and under a proper computer implementation of the formulation, a numerical solution should approach the exact solution upon refinement, and hence, the values of the total dissipation should decrease monotonically upon refinement. But these values are bounded below by the total dissipation under the exact solution, which again stems from the minimum dissipation theorem. The mentioned lower bound will be the plateau that the values of the total dissipation under numerical solutions reach.

The above reasoning also reveals that if the convergence of the total dissipation is not monotonic with refinement, then one of the hypotheses of the minimum dissipation theorem should have been violated. To put it differently, if the convergence is not monotonic or there is no convergence at all, one should suspect that there could be significant errors in satisfying the local mass balance condition (7.2) or in the implementation of boundary conditions.

7.2. *A posteriori* criterion based on reciprocal relations. Under the reciprocal relation of the double porosity/permeability model, if $(\mathbf{u}_1^{'}, p_1^{'}, \mathbf{u}_2^{'}, p_2^{'})$ and $(\mathbf{u}_1^*, p_1^*, \mathbf{u}_2^*, p_2^*)$ are, respectively, the *exact solutions* under prescribed data-sets $(\mathbf{b}^{'}, u_{n1}^{'}, p_{01}^{'}, u_{n2}^{'}, p_{02}^{'})$ and $(\mathbf{b}^*, u_{n1}^*, p_{01}^*, u_{n2}^*, p_{02}^*)$, then the

pair of exact solutions and the pair of prescribed data-sets satisfy the following relation [Nakshatrala et al., 2016]:

$$\begin{aligned}
&\int_\Omega \gamma \mathbf{b}^{'}(\mathbf{x}) \cdot \mathbf{u}_1^*(\mathbf{x}) \, \mathrm{d}\Omega - \int_{\Gamma_1^p} p_{01}^{'}(\mathbf{x}) \mathbf{u}_1^*(\mathbf{x}) \cdot \widehat{\mathbf{n}}(\mathbf{x}) \, \mathrm{d}\Gamma - \int_{\Gamma_1^u} p_1^{'}(\mathbf{x}) u_{n1}^*(\mathbf{x}) \, \mathrm{d}\Gamma \\
&+ \int_\Omega \gamma \mathbf{b}^{'}(\mathbf{x}) \cdot \mathbf{u}_2^*(\mathbf{x}) \, \mathrm{d}\Omega - \int_{\Gamma_2^p} p_{02}^{'}(\mathbf{x}) \mathbf{u}_2^*(\mathbf{x}) \cdot \widehat{\mathbf{n}}(\mathbf{x}) \, \mathrm{d}\Gamma - \int_{\Gamma_2^u} p_2^{'}(\mathbf{x}) u_{n2}^*(\mathbf{x}) \, \mathrm{d}\Gamma \\
&= \int_\Omega \gamma \mathbf{b}^{*}(\mathbf{x}) \cdot \mathbf{u}_1^{'}(\mathbf{x}) \, \mathrm{d}\Omega - \int_{\Gamma_1^p} p_{01}^{*}(\mathbf{x}) \mathbf{u}_1^{'}(\mathbf{x}) \cdot \widehat{\mathbf{n}}(\mathbf{x}) \, \mathrm{d}\Gamma - \int_{\Gamma_1^u} p_1^{*}(\mathbf{x}) u_{n1}^{'}(\mathbf{x}) \, \mathrm{d}\Gamma \\
&+ \int_\Omega \gamma \mathbf{b}^{*}(\mathbf{x}) \cdot \mathbf{u}_2^{'}(\mathbf{x}) \, \mathrm{d}\Omega - \int_{\Gamma_2^p} p_{02}^{*}(\mathbf{x}) \mathbf{u}_2^{'}(\mathbf{x}) \cdot \widehat{\mathbf{n}}(\mathbf{x}) \, \mathrm{d}\Gamma - \int_{\Gamma_2^u} p_2^{*}(\mathbf{x}) u_{n2}^{'}(\mathbf{x}) \, \mathrm{d}\Gamma
\end{aligned} \tag{7.3}$$

Unlike the minimum dissipation theorem, the reciprocal relation does not require the velocity boundary conditions to be prescribed on the entire boundary of the two pore-networks. However, the domain, Ω, and the boundaries, Γ_1^u, Γ_1^p, Γ_2^u, and Γ_2^p, are considered to be the same for prescribed data-sets. Also the reciprocal relation under the double porosity/permeability model does not require the set of solutions to be kinematically admissible.

It is important to note that numerical solutions do not possess reciprocal relations. There will always be an error under numerical solutions with respect to the reciprocal relation (7.3). However, this error can be quantified, and a way to achieve this is by defining the following scalar quantity, which is a form of relative error:

$$\varepsilon_{\text{reciprocal}} := \frac{|\text{l.h.s of Eqn. (7.3)} - \text{r.h.s of Eqn. (7.3)}|}{\text{l.h.s of Eqn. (7.3)}} \tag{7.4}$$

For exact solutions, we will have $\varepsilon_{\text{reciprocal}} = 0$. For those problems in which left hand side of equation (7.3) vanishes, one can use an absolute error measure instead of this relative error measure. Thus, the magnitude of $\varepsilon_{\text{reciprocal}}$ will serve as a measure to assess the accuracy of a numerical formulation.

A description of the proposed *a posteriori* criterion based on the reciprocal relation is as follows: Solve the given boundary value problem under h- or p-refinements. For each case of refinement, evaluate the relative error $\varepsilon_{\text{reciprocal}}$ using the obtained numerical solution. Plot the values of $\varepsilon_{\text{reciprocal}}$ with respect to characteristic mesh size h for the case of h-refinement or degrees-of-freedom in the case of p-refinement. The values of $\varepsilon_{\text{reciprocal}}$ under the obtained numerical solutions should decrease monotonically and reach a plateau upon refinements. Similar to the case of *a posteriori* criterion based on the minimum dissipation theorem, the numerical results provided at the end of this section support this trend.

One can construct a plausible reasoning for the mentioned trend in $\varepsilon_{\text{reciprocal}}$ similar to the reasoning provided under the minimum dissipation theorem. Since the reciprocal relation does not require the velocity fields to be kinematically admissible (specifically, the velocity fields need not satisfy the local mass balance condition (7.2)), it is reasonable to conclude that if $\varepsilon_{\text{reciprocal}}$ does not decrease monotonically with refinement, then one should suspect that there could be significant errors in the implementation of boundary conditions.

7.3. Representative numerical results. To illustrate the performance and utility of the mentioned mechanics-based *a posteriori* criteria, we employ the pipe bend problem, which is widely used as a benchmark problem for flow through porous media [Aage et al., 2008; Borrvall and Petersson, 2003; Challis and Guest, 2009]. A pictorial description of the problem is shown in

TABLE 6. Data-sets for the pipe bend problem.

Case 1	Case 2
$L_x^{'} = 1.0$	$L_x^{*} = 1.0$
$L_y^{'} = 1.0$	$L_y^{*} = 1.0$
$\mu^{'} = 1.0$	$\mu^{*} = 1.0$
$\beta^{'} = 1.0$	$\beta^{*} = 1.0$
$k_1^{'} = 1.0$	$k_1^{*} = 1.0$
$k_2^{'} = 0.01$	$k_2^{*} = 0.01$
$\gamma \mathbf{b}^{'} = \{1.0, 1.0\}$	$\gamma \mathbf{b}^{*} = \{0.0, 0.0\}$
$u_{n1}^{'} = 100(y - 0.6)(0.8 - y)$ on Γ^u_{inflow}	$u_{n1}^{*} = 1.0$ on Γ^u_{inflow}
$u_{n1}^{'} = -100(x - 0.6)(0.8 - x)$ on $\Gamma^u_{\text{outflow}}$	$u_{n1}^{*} = -1.0$ on $\Gamma^u_{\text{outflow}}$
$u_{n1}^{'} = 0$ on the other parts of $\partial\Omega$	$u_{n1}^{*} = 0$ on the other parts of $\partial\Omega$
$u_{n2}^{'} = 0$ on $\partial\Omega$	$u_{n2}^{*} = 0$ on $\partial\Omega$

Figure 12. The computational domain is a unit square ($L = 1.0$). For the velocity boundary conditions, two different cases are considered. For the macro-pore network in case 1, an inflow parabolic velocity is enforced on a portion of the left boundary (denoted as Γ^u_{inflow}) while an outflow parabolic velocity is applied on a portion of the bottom boundary (denoted as $\Gamma^u_{\text{outflow}}$). In case 2, an inflow constant velocity is enforced on Γ^u_{inflow} while an outflow constant velocity is applied on $\Gamma^u_{\text{outflow}}$ for the macro-pore network. For both cases, the normal component of macro-velocity is prescribed to be zero on the rest of the boundary (i.e., $u_n(\mathbf{x}) = 0$). The normal component of micro-velocity in both data-sets ($u_{n2}^{'}$ and u_{n2}^{*}) is zero in the data-sets on the entire boundary. These sample data-sets are provided in Table 6.

Figure 13(a) shows how the deviation in dissipation varies with mesh refinement for the numerical solutions obtained using both data-sets. Under h-refinement, as the mesh size h decreases (or the total number of the elements increases), the deviation in the dissipation value decreases for both cases and the convergence is monotonic. This deviation can be further quantified using $\varepsilon_{\text{reciprocal}}$ under the double porosity/permeability model for the sample data-sets as shown in Figure 13(b). For different orders of interpolation, the error in reciprocal relation for the two sets of numerical solutions decreases monotonically with mesh refinement for this test problem which implies that the numerical solutions converge monotonically. As can be seen, by increasing the order of interpolation for the primary variables, the value of error is decreased and the numerical solutions get closer to the exact solutions of the model.

8. AN EXTENSION TO TRANSIENT ANALYSIS

The discussions and the results presented in the previous sections neglected transient flow behavior within the porous domain. However, unsteady flow characteristics are indispensable in a wide variety of applications such as the ones observed in aquifers and oil-bearing strata [Mongan, 1985], and composite manufacturing applications based on resin transfer molding [Nakshatrala et al., 2006; Pacquaut et al., 2012] where two different fibers are usually used, providing two different pathways for the fluid. In this section, the proposed mixed formulation is extended to the transient case. We first document the governing equations in a transient setting, which will have an unsteady term in the balance of momentum equation for each pore-network. A stabilized

mixed formulation is then derived for the transient case. Finally, the performance of the proposed formulation in the transient case will be illustrated using a representative example.

8.1. Unsteady governing equations. Same as before, we consider a bounded domain, $\Omega \subset \mathbb{R}^{nd}$, with a piecewise smooth boundary denoted by $\partial\Omega$. The time is denoted by $t \in [0, T]$, where T is the total time of interest. Darcy velocity (vector) fields in macro- and micro-pores at any spatial point $\mathbf{x}$ are denoted by $\mathbf{u}_1(\mathbf{x}, t)$ and $\mathbf{u}_2(\mathbf{x}, t)$ respectively, while macro- and micro-pressure (scalar) fields are denoted by $p_1(\mathbf{x}, t)$, and $p_2(\mathbf{x}, t)$. The specific body force can also depend on time and is denoted by $\mathbf{b}(\mathbf{x}, t)$. Assuming that the porosities in the two pore-networks do not change with time, the transient governing equations can be written as follows:

$$\rho_1 \frac{\partial \mathbf{u}_1}{\partial t} + \mu \mathbf{K}_1^{-1} \mathbf{u}_1 + \text{grad}[p_1] = \gamma \mathbf{b} \quad \text{in } \Omega \times (0, T) \tag{8.1a}$$

$$\rho_2 \frac{\partial \mathbf{u}_2}{\partial t} + \mu \mathbf{K}_2^{-1} \mathbf{u}_2 + \text{grad}[p_2] = \gamma \mathbf{b} \quad \text{in } \Omega \times (0, T) \tag{8.1b}$$

$$\text{div}[\mathbf{u}_1] = +\chi \quad \text{in } \Omega \times (0, T) \tag{8.1c}$$

$$\text{div}[\mathbf{u}_2] = -\chi \quad \text{in } \Omega \times (0, T) \tag{8.1d}$$

$$\mathbf{u}_1(\mathbf{x}, t) \cdot \widehat{\mathbf{n}}(\mathbf{x}) = u_{n1}(\mathbf{x}, t) \quad \text{on } \Gamma_1^u \times (0, T) \tag{8.1e}$$

$$\mathbf{u}_2(\mathbf{x}, t) \cdot \widehat{\mathbf{n}}(\mathbf{x}) = u_{n2}(\mathbf{x}, t) \quad \text{on } \Gamma_2^u \times (0, T) \tag{8.1f}$$

$$p_1(\mathbf{x}, t) = p_{01}(\mathbf{x}, t) \quad \text{on } \Gamma_1^p \times (0, T) \tag{8.1g}$$

$$p_2(\mathbf{x}, t) = p_{02}(\mathbf{x}, t) \quad \text{on } \Gamma_2^p \times (0, T) \tag{8.1h}$$

$$\mathbf{u}_1(\mathbf{x}, 0) = \mathbf{u}_{01}(\mathbf{x}) \quad \text{in } \Omega \tag{8.1i}$$

$$\mathbf{u}_2(\mathbf{x}, 0) = \mathbf{u}_{02}(\mathbf{x}) \quad \text{in } \Omega \tag{8.1j}$$

where $\mathbf{u}_{01}(\mathbf{x})$ and $\mathbf{u}_{02}(\mathbf{x})$ are the prescribed initial velocities within the domain. The definitions for the other symbols remain the same as before. It is understood that the quantities corresponding to these symbols will now depend on the time, expect for the unit outward normal, as the domain is fixed and does not evolve with respect to the time. We now derive a stabilized formulation for the mentioned transient governing equations under the double porosity/permeability model.

8.2. A stabilized mixed formulation for the transient case. We employ the method of horizontal lines (also known as the Rothe's method) [Rothe, 1930], which is different from the semi-discrete method (also known as the method of vertical lines) [Hughes, 1987]. Under the method of horizontal lines, a given partial differential equation (which depends on both space and time) is discretized temporally using a time-stepping scheme. This gives rise to another partial differential equation which depends only on the spatial coordinates, and can be further discretized spatially using the finite element method, the finite difference method or the finite volume method. On the other hand, under the semi-discrete method, the given spatially and temporally dependent partial differential equation is first spatially discretized, say, using the finite element method, giving rise to a system of ordinary differential equations; which can be numerically solved by employing a convenient time-stepping scheme.

Herein, we employ the backward Euler time stepping scheme for the temporal discretization of the transient governing equations under the method of horizontal lines. However, one can employ any other time-stepping scheme with a straightforward modification. The backward Euler is first-order accurate and unconditionally stable when applied to a linear system of ordinary differential

equations [Hairer et al., 1993]. The time interval of interest is discretized into $N+1$ time levels denoted as t_n $(n = 0, \cdots, N)$ by assuming uniform time steps ($\Delta t = t_n - t_{n-1}$); however, one can consider non-uniform time steps by applying simple modifications. For a given quantity $z(\mathbf{x}, t)$, the time discretized version at the instant of time t_n can be written as follows:

$$z^{(n)}(\mathbf{x}) \approx z(\mathbf{x}, t_n), \quad n = 0, \cdots, N \tag{8.2}$$

The resulting time discretized equations at time level $t = t_{n+1}$ under the method of horizontal lines using the backward Euler time-stepping scheme take the following form:

$$\rho_1 \frac{\mathbf{u}_1^{(n+1)} - \mathbf{u}_1^{(n)}}{\Delta t} + \mu \mathbf{K}_1^{-1} \mathbf{u}_1^{(n+1)} + \text{grad}[p_1^{(n+1)}] = \gamma \mathbf{b}^{(n+1)} \quad \text{in } \Omega \tag{8.3a}$$

$$\rho_2 \frac{\mathbf{u}_2^{(n+1)} - \mathbf{u}_2^{(n)}}{\Delta t} + \mu \mathbf{K}_2^{-1} \mathbf{u}_2^{(n+1)} + \text{grad}[p_2^{(n+1)}] = \gamma \mathbf{b}^{(n+1)} \quad \text{in } \Omega \tag{8.3b}$$

$$\text{div}[\mathbf{u}_1^{(n+1)}] = +\chi^{(n+1)} \quad \text{in } \Omega \tag{8.3c}$$

$$\text{div}[\mathbf{u}_2^{(n+1)}] = -\chi^{(n+1)} \quad \text{in } \Omega \tag{8.3d}$$

$$\mathbf{u}_1^{(n+1)}(\mathbf{x}) \cdot \widehat{\mathbf{n}}(\mathbf{x}) = u_{n1}(\mathbf{x}, t = t_{n+1}) \quad \text{on } \Gamma_1^u \tag{8.3e}$$

$$\mathbf{u}_2^{(n+1)}(\mathbf{x}) \cdot \widehat{\mathbf{n}}(\mathbf{x}) = u_{n2}(\mathbf{x}, t = t_{n+1}) \quad \text{on } \Gamma_2^u \tag{8.3f}$$

$$p_1^{(n+1)}(\mathbf{x}) = p_{01}^{(n+1)}(\mathbf{x}) = p_{01}(\mathbf{x}, t = t_{n+1}) \quad \text{on } \Gamma_1^p \tag{8.3g}$$

$$p_2^{(n+1)}(\mathbf{x}) = p_{02}^{(n+1)}(\mathbf{x}) = p_{02}(\mathbf{x}, t = t_{n+1}) \quad \text{on } \Gamma_2^p \tag{8.3h}$$

$$\mathbf{u}_1^{(0)}(\mathbf{x}) = \mathbf{u}_{01}(\mathbf{x}) \quad \text{in } \Omega \tag{8.3i}$$

$$\mathbf{u}_2^{(0)}(\mathbf{x}) = \mathbf{u}_{02}(\mathbf{x}) \quad \text{in } \Omega \tag{8.3j}$$

Equations (8.3a) and (8.3b) can be rearranged as follows:

$$\left(\frac{\rho_1}{\Delta t}\mathbf{I} + \mu \mathbf{K}_1^{-1}\right) \mathbf{u}_1^{(n+1)} + \text{grad}[p_1^{(n+1)}] = \gamma \left(\mathbf{b}^{(n+1)} + \frac{\phi_1}{\Delta t}\mathbf{u}_1^{(n)}\right) \quad \text{in } \Omega \tag{8.4a}$$

$$\left(\frac{\rho_2}{\Delta t}\mathbf{I} + \mu \mathbf{K}_2^{-1}\right) \mathbf{u}_2^{(n+1)} + \text{grad}[p_2^{(n+1)}] = \gamma \left(\mathbf{b}^{(n+1)} + \frac{\phi_2}{\Delta t}\mathbf{u}_2^{(n)}\right) \quad \text{in } \Omega \tag{8.4b}$$

where the (modified) drag coefficients and (modified) body forces can be written as follows:

$$\widehat{\alpha}_1 = \left(\frac{\rho_1}{\Delta t}\mathbf{I} + \mu \mathbf{K}_1^{-1}\right) \tag{8.5a}$$

$$\widehat{\alpha}_2 = \left(\frac{\rho_2}{\Delta t}\mathbf{I} + \mu \mathbf{K}_2^{-1}\right) \tag{8.5b}$$

$$\tilde{\mathbf{b}}_1^{(n+1)} = \left(\mathbf{b}^{(n+1)} + \frac{\phi_1}{\Delta t}\mathbf{u}_1^{(n)}\right) \tag{8.5c}$$

$$\tilde{\mathbf{b}}_2^{(n+1)} = \left(\mathbf{b}^{(n+1)} + \frac{\phi_2}{\Delta t}\mathbf{u}_2^{(n)}\right) \tag{8.5d}$$

where ϕ_1 and ϕ_2 are, respectively, the volume fractions associated with the two pore-networks, relating the bulk density and the true density as $\rho_i = \phi_i \gamma$ $(i = 1, 2)$.

The stabilized mixed formulation for the unsteady condition at time level $t = t_{n+1}$ reads as: Find $\left(\mathbf{u}_1^{(n+1)}(\mathbf{x}), \mathbf{u}_2^{(n+1)}(\mathbf{x})\right) \in \bar{\mathcal{U}}_{1,t=t_{n+1}} \times \bar{\mathcal{U}}_{2,t=t_{n+1}}$, and $\left(p_1^{(n+1)}(\mathbf{x}), p_2^{(n+1)}(\mathbf{x})\right) \in \bar{\mathcal{Q}}$ such that we have

$$\mathcal{B}_{\text{stab}}(\mathbf{w}_1, \mathbf{w}_2, q_1, q_2; \mathbf{u}_1^{(n+1)}, \mathbf{u}_2^{(n+1)}, p_1^{(n+1)}, p_2^{(n+1)}) = \mathcal{L}_{\text{stab}}^{\text{tran}}(\mathbf{w}_1, \mathbf{w}_2, q_1, q_2)$$

$$\forall\,(\mathbf{w}_1(\mathbf{x}),\mathbf{w}_2(\mathbf{x}))\ \in \bar{\mathcal{W}}_1\times\bar{\mathcal{W}}_2, (q_1(\mathbf{x}),q_2(\mathbf{x}))\in\bar{\mathcal{Q}} \tag{8.6}$$

The linear functional under the transient condition $\mathcal{L}^{\text{tran}}_{\text{stab}}(\mathbf{w}_1,\mathbf{w}_2,q_1,q_2)$ is slightly different from the one under the steady-state condition. Under the steady-state condition, the body forces, denoted by $\mathbf{b}(\mathbf{x})$, are similar in both pore-networks. However, for the transient case, body forces in the macro- and micro-pore networks ($\tilde{\mathbf{b}}_1^{(n+1)}$ and $\tilde{\mathbf{b}}_2^{(n+1)}$) are different and one should substitute $\mathbf{b}(\mathbf{x})$ in the $\mathcal{L}_{\text{stab}}(\mathbf{w}_1,\mathbf{w}_2,q_1,q_2)$ by the associated value in each pore-network in order to obtain $\mathcal{L}^{\text{tran}}_{\text{stab}}(\mathbf{w}_1,\mathbf{w}_2,q_1,q_2)$. It should also be noted that in the bilinear form and the linear functional of the proposed formulation provided in equations (3.8) and (3.9), $\mu\mathbf{K}_i^{-1}$ should be replaced by $\widehat{\alpha}_i,\ (i=1,2)$.

A systematic numerical implementation of the proposed formulation is outlined in Algorithm 1. It should be noted that, we need not evaluate all the terms in the variational form, especially the terms in $\mathcal{B}_{\text{stab}}$, at each time step since most of them do not depend on the temporal variable. Therefore, it is enough to only evaluate the terms involving $\tilde{\mathbf{b}}_i^{(n+1)},\ i=1,2$ in the $\mathcal{L}^{\text{tran}}_{\text{stab}}$ repeatedly.

Algorithm 1 Implementation of the proposed formulation.

1: Inputs: Initial conditions $\mathbf{u}_{01}$ and $\mathbf{u}_{02}$, time period of integration T, maximum allowable time step $\Delta t_{\max}$
2: Set $\mathbf{u}_1^{(n)}=\mathbf{u}_{01}$ and $\mathbf{u}_2^{(n)}=\mathbf{u}_{02}$
3: Set $t=0$
4: **while** $t<T$ **do**
5: $\quad\Delta t=\min[\Delta t_{\max},T-t],\ t=t+\Delta t$
6: $\quad$Using $\mathbf{u}_1^{(n)}$ and $\mathbf{u}_2^{(n)}$, solve equation (8.6) to obtain $\mathbf{u}_1^{(n+1)}$, $\mathbf{u}_2^{(n+1)}$, $p_1^{(n+1)}$, and $p_2^{(n+1)}$
7: $\quad$Set $\mathbf{u}_1^{(n)}=\mathbf{u}_1^{(n+1)}$ and $\mathbf{u}_2^{(n)}=\mathbf{u}_2^{(n+1)}$
8: **end while**

The relevant function spaces for the velocity and pressure fields and their corresponding weighting functions under the transient case are defined as follows:

$$\bar{\mathcal{U}}_{1,t}:=\left\{\mathbf{u}_1(\mathbf{x})\in(L_2(\Omega))^{nd}\ \middle|\ \text{div}[\mathbf{u}_1]\in L_2(\Omega),\mathbf{u}_1(\mathbf{x})\cdot\widehat{\mathbf{n}}(\mathbf{x})=u_{n1}(\mathbf{x},t)\text{ on }\Gamma_1^u\right\} \tag{8.7a}$$

$$\bar{\mathcal{U}}_{2,t}:=\left\{\mathbf{u}_2(\mathbf{x})\in(L_2(\Omega))^{nd}\ \middle|\ \text{div}[\mathbf{u}_2]\in L_2(\Omega),\mathbf{u}_2(\mathbf{x})\cdot\widehat{\mathbf{n}}(\mathbf{x})=u_{n2}(\mathbf{x},t)\text{ on }\Gamma_2^u\right\} \tag{8.7b}$$

$$\bar{\mathcal{W}}_1:=\left\{\mathbf{w}_1(\mathbf{x})\in(L_2(\Omega))^{nd}\ \middle|\ \text{div}[\mathbf{w}_1]\in L_2(\Omega),\mathbf{w}_1(\mathbf{x})\cdot\widehat{\mathbf{n}}(\mathbf{x})=0\text{ on }\Gamma_1^u\right\} \tag{8.7c}$$

$$\bar{\mathcal{W}}_2:=\left\{\mathbf{w}_2(\mathbf{x})\in(L_2(\Omega))^{nd}\ \middle|\ \text{div}[\mathbf{w}_2]\in L_2(\Omega),\mathbf{w}_2(\mathbf{x})\cdot\widehat{\mathbf{n}}(\mathbf{x})=0\text{ on }\Gamma_2^u\right\} \tag{8.7d}$$

$$\bar{\mathcal{Q}}:=\left\{(p_1(\mathbf{x}),p_2(\mathbf{x}))\in H^1(\Omega)\times H^1(\Omega)\ \middle|\ \left(\int_\Omega p_1(\mathbf{x})\mathrm{d}\Omega\right)\left(\int_\Omega p_2(\mathbf{x})\mathrm{d}\Omega\right)=0\right\} \tag{8.7e}$$

8.3. A representative numerical example. We now illustrate the performance of the proposed stabilized mixed formulation for studying transient flow problems using a two-dimensional problem. Moreover, some unique features of flows in porous media exhibiting two distinct pore-networks are illustrated.

The computational domain Ω is chosen to be the region in-between a rectangle of length 10.0 and height 1.0 and two square holes each of length 0.4. Zero-flux boundary conditions for both macro-pore and micro-pore networks are prescribed at the holes as well as top and bottom edges of the rectangular domain. At the right end, pressure is prescribed at both pore-networks. At the left end, however, zero-flux boundary condition is prescribed for the micro-pore network and pressure is

prescribed for the macro-pore network. The initial velocities for both fluid constituents are assumed to be zero. A pictorial description of the domain as well as the initial and boundary conditions are illustrated in Figure 14. Table 7 provides the parameter values for the two-dimensional transient flow problem.

TABLE 7. Data-set for two-dimensional transient flow problem.

Parameter	Value
$\gamma\mathbf{b}$	$\{0.0, 0.0\}$
L_x	10.0
L_y	1.0
L_{hole}	0.4
μ	1.0
β	1.0
k_1	10000
k_2	1.0
p_1^L	$10\ \sin(0.4(y + 2.0t))$
p_1^R	10.0
p_2^R	10.0
u_{n2}^L	0.0
u_{n2}^R	0.0
u_{01}	0.0
u_{02}	0.0
Δt	$5\text{e} - 11$
T	$6\text{e} - 8$

Figure 15 shows a comparison between macro-velocity ($\mathbf{u}_1$) and micro-velocity ($\mathbf{u}_2$) at selected time steps. *As can be seen in this figure, the rate of decay of the solution in the macro-pore network (which has a higher permeability than the micro-pore network) is slower than that of the micro-pore network, and hence, the micro-velocity reaches the steady-state faster than the macro-velocity.* This is not counterintuitive if one realizes that the rate of dissipation in a pore-network is inversely proportional to the permeability of the pore-network. Specifically, the rates of dissipation in macro- and micro-pore networks under the double porosity/permeability model are, respectively, defined as follows [Nakshatrala et al., 2016]:

$$\mu\mathbf{K}_1^{-1}\mathbf{u}_1 \cdot \mathbf{u}_1 \quad \text{and} \quad \mu\mathbf{K}_2^{-1}\mathbf{u}_2 \cdot \mathbf{u}_2$$

It is also noteworthy to recall the definition of permeability of a porous medium, which is a measure of the ability of the porous medium to transmit fluids through it. To put it differently, the greater is the permeability the lesser will be resistance offered by the pore-network, and hence the greater will be the ease with which a fluid flows through the pore-network.

9. COUPLED PROBLEMS

Experimental studies on Darcy flow coupled with transport problem have revealed the possibility of occurrence of certain physical instabilities called Saffman-Taylor instability [Chuoke et al., 1959; Saffman and Taylor, 1958]. In the miscible displacement of fluids in porous media with a single pore-network, a more viscous fluid is displaced by a less viscous fluid within the domain [Homsy, 1987; Stalkup, 1983]. Imposing any disturbance or perturbation on the interface of the

two fluids leads to appearance of finger-like patterns at the interface of the two fluids due to the penetration of the less viscous fluid into the more viscous one. This type of physical instability, which is commonly observed in a wide variety of industrial and environmental applications such as carbon-dioxide sequestration and secondary and tertiary oil recovery, is also referred to as viscous fingering (VF) instability [Chen and Meiburg, 1998a,b; Homsy, 1987].

All the existing theoretical and numerical studies in the literature are available for the *classical* Saffman-Taylor instability. The questions remaining are whether similar physical instabilities can be captured under the double porosity/permeability model and if so, how the flow model can affect the mechanism of the instabilities and their characteristics (i.e., number of fingers, their characteristic length, growth rate, scaling laws, etc.). Herein, we cannot provide an exhaustive study on such well-known instabilities in fluid mechanics and many important areas of research associated with viscous fingering are not included in our discussion. Therefore, we only address the former question by studying the possibility of occurrence of Saffman-Taylor-type instabilities under the double porosity/permeability model. The proposed stabilized formulation will be employed for modeling double porosity/permeability model coupled with transport problem to illustrate the capability of the proposed computational framework for capturing Saffman-Taylor-type instabilities within a porous domain exhibiting double pore-networks. However, studying the effects of the flow model (double porosity/permeability model versus Darcy model) on the mode and patterns of the instabilities is beyond the scope of this paper and will be addressed in a separate paper.

9.1. Governing equations: Coupled flow and transport problem. Viscous fingering can be considered as a two-way coupled flow and transport problem and is studied in the Hele-Shaw cell. The governing equations can be written as follows:

$$\mu\mathbf{K}_1^{-1}\mathbf{u}_1(\mathbf{x},t) + \text{grad}[p_1(\mathbf{x},t)] = \gamma\mathbf{b}(\mathbf{x},t) \qquad \text{in } \Omega\times(0,T) \qquad (9.1a)$$

$$\mu\mathbf{K}_2^{-1}\mathbf{u}_2(\mathbf{x},t) + \text{grad}[p_2(\mathbf{x},t)] = \gamma\mathbf{b}(\mathbf{x},t) \qquad \text{in } \Omega\times(0,T) \qquad (9.1b)$$

$$\text{div}[\mathbf{u}_1(\mathbf{x},t)] = +\chi(\mathbf{x},t) \qquad \text{in } \Omega\times(0,T) \qquad (9.1c)$$

$$\text{div}[\mathbf{u}_2(\mathbf{x},t)] = -\chi(\mathbf{x},t) \qquad \text{in } \Omega\times(0,T) \qquad (9.1d)$$

$$\mathbf{u}_1(\mathbf{x},t)\cdot\widehat{\mathbf{n}}(\mathbf{x}) = u_{n1}(\mathbf{x},t) \qquad \text{on } \Gamma_1^u\times(0,T) \qquad (9.1e)$$

$$\mathbf{u}_2(\mathbf{x},t)\cdot\widehat{\mathbf{n}}(\mathbf{x}) = u_{n2}(\mathbf{x},t) \qquad \text{on } \Gamma_2^u\times(0,T) \qquad (9.1f)$$

$$p_1(\mathbf{x},t) = p_{01}(\mathbf{x},t) \qquad \text{on } \Gamma_1^p\times(0,T) \qquad (9.1g)$$

$$p_2(\mathbf{x},t) = p_{02}(\mathbf{x},t) \qquad \text{on } \Gamma_2^p\times(0,T) \qquad (9.1h)$$

$$\frac{\partial c(\mathbf{x},t)}{\partial t} + \text{div}\left[\mathbf{u}(\mathbf{x},t)c(\mathbf{x},t) - \mathbf{D}(\mathbf{x},t)\text{grad}[c(\mathbf{x},t)]\right] = f(\mathbf{x},t) \qquad \text{in } \Omega\times(0,T) \qquad (9.1i)$$

$$c(\mathbf{x},t) = c^p(\mathbf{x},t) \qquad \text{on } \Gamma^D\times(0,T) \qquad (9.1j)$$

$$\widehat{\mathbf{n}}(\mathbf{x})\cdot(\mathbf{u}(\mathbf{x},t)c(\mathbf{x},t) - \mathbf{D}(\mathbf{x},t)\text{grad}[c(\mathbf{x},t)]) = q^p(\mathbf{x},t) \qquad \text{on } \Gamma^N\times(0,T) \qquad (9.1k)$$

$$c(\mathbf{x},t=0) = c_0(\mathbf{x}) \qquad \text{in } \Omega \qquad (9.1l)$$

where equations (9.1a) – (9.1h) represent the flow equations under the double porosity/permeability model, and equations (9.1i) – (9.1l) represent the transient advection-diffusion problem. Herein, $c(\mathbf{x},t)$ denotes the concentration and $\mathbf{D}(\mathbf{x},t)$ is the diffusivity tensor.

In order to assure the proper coupling between flow problem and the transient advection-diffusion problem, the viscosity is assumed to exponentially depend on the concentration as follows:

$$\mu(c(\mathbf{x},t)) = \mu_0 \exp\left[R_c(1 - c(\mathbf{x},t))\right] \tag{9.2}$$

where μ_0 is the base viscosity and R_c denotes the log-mobility ratio in an isothermal miscible displacement. Figure 16 represents the computational domain as well as the assigned initial and boundary conditions for this boundary value problem. Parameter values for this coupled flow and transport problem are provided in Table 8. The perturbation on the interface of the two fluids is imposed by considering heterogeneous material properties for the porous domain, such as heterogeneous permeabilities. Moreover, the initial condition for the transport problem is defined using a random function throughout the domain.

TABLE 8. Data-set for coupled flow and transport problem.

Parameter	Value
$\gamma\mathbf{b}$	$\{0.0, 0.0\}$
f	0.0
L_x	1.0
L_y	0.4
μ_0	0.001
R_c	3.0
D	$2\mathrm{e}-6$
β	1.0
$\mathbf{K}_1$	$[1.0, 0.0; 0.0, 0.5]$
$\mathbf{K}_2$	$[0.05, 0.0; 0.0, 0.01]$
c_0	0.0
c_{inj}	1.0
p_{atm}	1.0
u_{inj}	0.004
Δt	0.5
T	150

Figure 17 shows the concentration profile under the double porosity/permeability model. Two main inferences can be drawn from this figure. *First*, Saffman-Taylor-type physical instability can *also* occur under the double porosity/permeability model. As discussed earlier, the classical Saffman-Taylor instability has been shown to occur under the Darcy model. However, a further systematic study needs to be conducted to find out the similarities and differences between the classical Saffman-Taylor instability and the one under the double porosity/permeability model. *Second*, the proposed stabilized formulation is capable of eliminating the spurious numerical instabilities without suppressing the underlying physical instability. Achieving this important attribute under the proposed stabilized formulation is one of the main contributions of this paper, as it has been shown recently that some stabilized formulations (for example, the Streamline/Upwind Petrov Galerkin (SUPG), and Galerkin Least-Squares (GLS) formulations) which are commonly used to suppress spurious numerical instabilities, may also suppress physical instabilities in some cases [Shabouei, 2016; Shabouei and Nakshatrala].

10. CONCLUDING REMARKS

This paper has made several contributions to the modeling of fluid flow in porous media with dual pore-networks and possible mass transfer across the pore-networks. *First*, a stabilized mixed finite element formulation has been presented for the double porosity/permeability mathematical model. *Second*, a systematic error analysis has been performed on the proposed stabilized weak formulation. Numerical convergence analysis and patch tests have been used to illustrate the convergence behavior and accuracy of the proposed mixed formulation in the discrete setting. *Third*, the mathematical properties that the solutions of the double porosity/permeability model enjoy have been utilized to construct mechanics-based *a posteriori* error measures to assess the accuracy of the numerical solutions. *Last but not least*, the performance of the proposed stabilized mixed formulation for modeling the transient flow as well as coupled problems has been illustrated using representative numerical examples. Some of the significant findings of this paper can be summarized as follows:

(C1) Equal-order interpolation for all the field variables (pressure and velocity vector fields), which is computationally the most convenient, is stable under the proposed stabilized mixed formulation.

(C2) Patch tests revealed that the classical mixed formulation produces spurious node-to-node oscillations in the pressure fields under equal-order interpolation for all the field variables. The proposed stabilized mixed formulation was able to eliminate such unphysical oscillations in the pressure fields, and passed the patch tests up to the machine precision.

(C3) The numerical convergence rates obtained using the proposed stabilized formulation were in accordance with the theory for both h- and p-refinements.

(C4) The accuracy of numerical solutions was assessed using the mechanics-based *a posteriori* error measures for the pipe bend problem. The errors decreased *monotonically* with mesh refinement for different orders of interpolation. This implies that the stabilized formulation is convergent and the computer implementation is correct. It should be noted that the mechanics-based solution verification method can be applied to any problem with any boundary condition.

(C5) An extension of the proposed formulation to the transient case has performed well, as it was able to predict accurately that the rate of decay of the response (e.g., the velocity front) in the macro-pore network is slower than that of the micro-pore network. Physically, this phenomenon of slower decay can be attributed to the higher permeability (which implies lower dissipation, as dissipation is inversely proportional to the permeability) in the macro-pore network.

(C6) The proposed stabilized mixed formulation suppressed the unphysical numerical instabilities but yet captured the underlying physical instability when applied to a coupled flow and transport problem in porous media with dual pore-networks. The captured physical instability, is similar to the classical Saffman-Taylor instability that has been shown to exist for coupled Darcy and transport equations. The proposed formulation will be particularly attractive for studying physical instabilities, as it has been shown recently that some well-known stabilized formulations which are designed to suppress numerical instabilities also suppressed physical instabilities.

The research presented herein can be extended on three fronts.

(R1) One can develop a hierarchy of mathematical models by incorporating other processes into the double porosity/permeability model. For example, the flow of multi-phase fluids in porous media exhibiting double porosity/permeability, and the incorporation of deformation of porous solid.

(R2) One can perform a theoretical study on the Saffman-Taylor-type instabilities under the double porosity/permeability model. In particular, one can address whether there are additional instability modes under the double porosity/permeability model when compared with the classical Saffman-Taylor instability (which is based on the Darcy model). One can also obtain scaling laws.

(R3) Heterogeneity of material properties and discontinuous distribution of permeability are very common in subsurface formations. Studies for the case of Darcy equations have shown that continuous formulations cannot properly handle abrupt changes in material properties, as the numerical solutions suffer from Gibbs phenomenon (which manifests as spurious oscillations in the numerical solution fields) [Hughes et al., 2006]. Thus one can develop a stabilized mixed discontinuous Galerkin formulation for the double porosity/permeability model that does not suffer from the Gibbs phenomenon in the solution fields when applied to problems with disparate medium properties.

Appendix A. Derivation of the proposed stabilized formulation

We provide a formal mathematical derivation of the proposed stabilized mixed weak formulation. We employ the variational multiscale paradigm [Hughes, 1995], and obtain the stabilization terms and the stabilization parameter in a consistent manner. Such an approach has been successfully employed to develop stabilized formulations for porous media models with single pore-network; for example, see [Hughes et al., 2006; Masud and Hughes, 2002; Nakshatrala et al., 2006]. The basic idea is to decompose the solution into resolved and unresolved components, estimate the unresolved component, and substitute the estimated component into the weak form to obtain the proposed stabilized mixed formulation. By a resolved component, we refer to that part of the solution that is captured by the underlying formulation (which, in our case, is the classical mixed formulation). The unresolved component can be interpreted as the difference between the exact solution and the resolved component. To improve the accuracy of the numerical solution, the unresolved components need to be estimated accurately, which can be achieved using the variational multiscale paradigm.

We start our derivation by decomposing the macro-scale and micro-scale velocities into resolved and unresolved components. Mathematically,

$$\mathbf{u}_1(\mathbf{x}) = \underbrace{\overline{\mathbf{u}}_1(\mathbf{x})}_{\text{resolved}} + \underbrace{\mathbf{u}_1^{'}(\mathbf{x})}_{\text{unresolved}} \quad \text{and} \quad \mathbf{u}_2(\mathbf{x}) = \underbrace{\overline{\mathbf{u}}_2(\mathbf{x})}_{\text{resolved}} + \underbrace{\mathbf{u}_2^{'}(\mathbf{x})}_{\text{unresolved}} \tag{A.1}$$

where the resolved components are denoted by over-lines, and the primed quantities represent the unresolved components. Similarly, the weighting functions corresponding to these velocities are decomposed as follows:

$$\mathbf{w}_1(\mathbf{x}) = \overline{\mathbf{w}}_1(\mathbf{x}) + \mathbf{w}_1^{'}(\mathbf{x}) \quad \text{and} \quad \mathbf{w}_2(\mathbf{x}) = \overline{\mathbf{w}}_2(\mathbf{x}) + \mathbf{w}_2^{'}(\mathbf{x}) \tag{A.2}$$

In principle, one could perform a similar decomposition to the macro- and micro-pressure fields. Herein, we assume that the pressure fields will be adequately resolved. Therefore, we do not decompose the pressure fields (i.e., $p_1(\mathbf{x})$ and $p_2(\mathbf{x})$) and the corresponding weighting functions (i.e., $q_1(\mathbf{x})$ and $q_2(\mathbf{x})$). In Sections 4 and 5, we have illustrated, through stability analysis and numerical

simulations, that such an assumption is still able to provide a stable and accurate formulation. To localize the unresolved components, we enforce the closure conditions that the unresolved components of the velocities and their weighting functions vanish on the element boundaries. That is,

$$\mathbf{u}_1^{'}(\mathbf{x}) = \mathbf{0}, \quad \mathbf{u}_2^{'}(\mathbf{x}) = \mathbf{0}, \quad \mathbf{w}_1^{'}(\mathbf{x}) = \mathbf{0} \quad \text{and} \quad \mathbf{w}_2^{'}(\mathbf{x}) = \mathbf{0} \quad \text{on } \partial\Omega^e;\ e = 1, \cdots, Nele \tag{A.3}$$

By substituting the multiscale decompositions given by equations (A.1) an (A.2) into the classical mixed formulation given in equation (3.4), invoking the arbitrariness of the weighting functions ($\overline{\mathbf{w}}(\mathbf{x})$ and $\mathbf{w}^{'}(\mathbf{x})$), and enforcing the closure conditions given by equation (A.3), we obtain two subproblems for each pore-network. The two subproblems corresponding to the macro-pore network can be written as follows:

$$(\overline{\mathbf{w}}_1; \mu\mathbf{K}_1^{-1}\overline{\mathbf{u}}_1 + \mu\mathbf{K}_1^{-1}\mathbf{u}_1^{'}) - (\text{div}[\overline{\mathbf{w}}_1]; p_1) + (q_1; \text{div}[\overline{\mathbf{u}}_1] + \text{div}[\mathbf{u}_1^{'}]) + (q_1; \beta/\mu(p_1 - p_2)) = (\overline{\mathbf{w}}_1; \gamma\mathbf{b}) - \langle \overline{\mathbf{w}}_1 \cdot \widehat{\mathbf{n}}; p_{01} \rangle_{\Gamma_1^{\text{p}}} \tag{A.4a}$$

$$(\mathbf{w}_1^{'}; \mu\mathbf{K}_1^{-1}\overline{\mathbf{u}}_1 + \mu\mathbf{K}_1^{-1}\mathbf{u}_1^{'})_{\Omega^e} - (\text{div}[\mathbf{w}_1^{'}]; p_1)_{\Omega^e} = (\mathbf{w}_1^{'}; \gamma\mathbf{b})_{\Omega^e} \quad \forall e = 1, \cdots, Nele \tag{A.4b}$$

The two subproblems corresponding to the micro-pore network can be written as follows:

$$(\overline{\mathbf{w}}_2; \mu\mathbf{K}_2^{-1}\overline{\mathbf{u}}_2 + \mu\mathbf{K}_2^{-1}\mathbf{u}_2^{'}) - (\text{div}[\overline{\mathbf{w}}_2]; p_2) + (q_2; \text{div}[\overline{\mathbf{u}}_2] + \text{div}[\mathbf{u}_2^{'}]) - (q_2; \beta/\mu(p_1 - p_2)) = (\overline{\mathbf{w}}_2; \gamma\mathbf{b}) - \langle \overline{\mathbf{w}}_2 \cdot \widehat{\mathbf{n}}; p_{02} \rangle_{\Gamma_2^{\text{p}}} \tag{A.5a}$$

$$(\mathbf{w}_2^{'}; \mu\mathbf{K}_2^{-1}\overline{\mathbf{u}}_2 + \mu\mathbf{K}_2^{-1}\mathbf{u}_2^{'})_{\Omega^e} - (\text{div}[\mathbf{w}_2^{'}]; p_2)_{\Omega^e} = (\mathbf{w}_2^{'}; \gamma\mathbf{b})_{\Omega^e} \quad \forall e = 1, \cdots, Nele \tag{A.5b}$$

We enforce the closure conditions using bubble functions, which vanish on the boundary of the domain on which they are defined [Baiocchi et al., 1993]. We, therefore, mathematically write the unresolved quantities as follows:

$$\mathbf{u}_1^{'}(\mathbf{x}) = b^e(\mathbf{x})\boldsymbol{\xi}_1,\ \mathbf{w}_1^{'}(\mathbf{x}) = b^e(\mathbf{x})\boldsymbol{\zeta}_1,\ \mathbf{u}_2^{'}(\mathbf{x}) = b^e(\mathbf{x})\boldsymbol{\xi}_2 \quad \text{and} \quad \mathbf{w}_2^{'}(\mathbf{x}) = b^e(\mathbf{x})\boldsymbol{\zeta}_2 \quad \forall \mathbf{x} \in \Omega^e \tag{A.6}$$

where $\boldsymbol{\xi}_1$, $\boldsymbol{\xi}_2$, $\boldsymbol{\zeta}_1$ and $\boldsymbol{\zeta}_2$ are constant vectors independent of $\mathbf{x}$, and $b^e(\mathbf{x})$ is a bubble function defined on the element Ω^e. By substituting equation (A.6) into the subproblems given by equations (A.4b) and (A.5b), and noting that $\boldsymbol{\zeta}_1$ and $\boldsymbol{\zeta}_2$ are arbitrary vectors; we estimate the unresolved velocities as follows:

$$\mathbf{u}_1^{'}(\mathbf{x}) = -b^e(\mathbf{x}) \left(\int_{\Omega^e} (b^e(\mathbf{x}))^2 \, d\Omega \right)^{-1} \int_{\Omega^e} b^e(\mathbf{y}) \overline{\mathbf{r}}_1(\mathbf{y}) d\Omega_{\mathbf{y}} \tag{A.7a}$$

$$\mathbf{u}_2^{'}(\mathbf{x}) = -b^e(\mathbf{x}) \left(\int_{\Omega^e} (b^e(\mathbf{x}))^2 \, d\Omega \right)^{-1} \int_{\Omega^e} b^e(\mathbf{y}) \overline{\mathbf{r}}_2(\mathbf{y}) d\Omega_{\mathbf{y}} \tag{A.7b}$$

where the residuals of the resolved quantities for the macro and micro pore-networks are, respectively, defined as follows:

$$\overline{\mathbf{r}}_1(\mathbf{x}) = \overline{\mathbf{u}}_1(\mathbf{x}) + \frac{1}{\mu}\mathbf{K}_1 \left(\text{grad}[p_1] - \gamma\mathbf{b}(\mathbf{x}) \right) \tag{A.8}$$

$$\overline{\mathbf{r}}_2(\mathbf{x}) = \overline{\mathbf{u}}_2(\mathbf{x}) + \frac{1}{\mu}\mathbf{K}_2 \left(\text{grad}[p_2] - \gamma\mathbf{b}(\mathbf{x}) \right) \tag{A.9}$$

Since in a finite element setting, the residuals ($\overline{\mathbf{r}}_1(\mathbf{x})$ and $\overline{\mathbf{r}}_2(\mathbf{x})$) are essentially constant over an element in the limit of an adequately refined mesh, the velocities in equations (A.7a) and (A.7b) can be written as follows:

$$\mathbf{u}_1^{'}(\mathbf{x}) = -\tau(\mathbf{x})\overline{\mathbf{r}}_1(\mathbf{x}) \quad \text{and} \quad \mathbf{u}_2^{'}(\mathbf{x}) = -\tau(\mathbf{x})\overline{\mathbf{r}}_2(\mathbf{x}) \tag{A.10}$$

where the stabilization parameter $\tau(\mathbf{x})$ takes the following form:

$$\tau(\mathbf{x}) = b^e(\mathbf{x}) \left(\int_{\Omega^e} \left(b^e(\mathbf{x})\right)^2 d\Omega \right)^{-1} \left(\int_{\Omega^e} b^e(\mathbf{x}) d\Omega \right) \tag{A.11}$$

One can employ the above stabilization parameter for obtaining a stabilized formulation. However, for the double porosity/permeability model it is adequate to employ a representative value for the stabilization parameter, which is justified by the convergence analysis we presented in this paper. To obtain a representative value for the stabilization parameter, we consider the average of $\tau(\mathbf{x})$, which can be written as follows:

$$\tau_{\text{avg}} = \frac{1}{\text{meas}(\Omega^e)} \int_{\Omega^e} \tau(\mathbf{x}) d\Omega = \left(\int_{\Omega^e} \left(b^e(\mathbf{x})\right)^2 d\Omega \right)^{-1} \left(\int_{\Omega^e} b^e(\mathbf{x}) d\Omega \right)^2 \tag{A.12}$$

where $\text{meas}(\Omega^e)$ denotes the measure of Ω^e (By measure we mean length in 1D, area in 2D and volume in 3D.) It has been shown in [Nakshatrala et al., 2006] that it is possible to construct a bubble function that gives a value of one-half for τ_{avg} for a given Ω^e. We thus take one-half to be the representative value for the stabilization parameter. We then approximate the unresolved components of the velocities as follows:

$$\mathbf{u}_1^{'}(\mathbf{x}) \approx -\frac{1}{2}\bar{\mathbf{r}}_1(\mathbf{x}) \quad \text{and} \quad \mathbf{u}_2^{'}(\mathbf{x}) \approx -\frac{1}{2}\bar{\mathbf{r}}_2(\mathbf{x}) \tag{A.13}$$

By substituting the above expressions into the subproblems given by equations (A.4a) and (A.5a), and noting the definitions for $\bar{\mathbf{r}}_1(\mathbf{x})$ and $\bar{\mathbf{r}}_2(\mathbf{x})$, we obtain a stabilized formulation of the following form:

$$\begin{aligned}
&\mathcal{B}_{\text{Gal}}(\overline{\mathbf{w}}_1, \overline{\mathbf{w}}_2, q_1, q_2; \overline{\mathbf{u}}_1, \overline{\mathbf{u}}_2, p_1, p_2) - \frac{1}{2}\left(\mu \mathbf{K}_1^{-1} \overline{\mathbf{w}}_1 - \text{grad}[q_1]; \overline{\mathbf{u}}_1 + \frac{1}{\mu}\mathbf{K}_1 \text{grad}[p_1] \right) \\
&\qquad -\frac{1}{2}\left(\mu \mathbf{K}_2^{-1} \overline{\mathbf{w}}_2 - \text{grad}[q_2]; \overline{\mathbf{u}}_2 + \frac{1}{\mu}\mathbf{K}_2 \text{grad}[p_2] \right) = \mathcal{L}_{\text{Gal}}(\overline{\mathbf{w}}_1, \overline{\mathbf{w}}_2, q_1, q_2) \\
&-\frac{1}{2}\left(\mu \mathbf{K}_1^{-1} \overline{\mathbf{w}}_1 - \text{grad}[q_1]; \frac{1}{\mu}\mathbf{K}_1 \gamma \mathbf{b} \right) - \frac{1}{2}\left(\mu \mathbf{K}_2^{-1} \overline{\mathbf{w}}_2 - \text{grad}[q_2]; \frac{1}{\mu}\mathbf{K}_2 \gamma \mathbf{b} \right)
\end{aligned} \tag{A.14}$$

where $\mathcal{B}_{\text{Gal}}$ and $\mathcal{L}_{\text{Gal}}$ are defined in equations (3.5) and (3.6), respectively. It should be noted that all the quantities in the above equation are resolved components. We therefore drop the over-lines for convenience, and write the above stabilized mixed formulation in the following compact form:

$$\begin{aligned}
&\mathcal{B}_{\text{stab}}(\mathbf{w}_1, \mathbf{w}_2, q_1, q_2; \mathbf{u}_1, \mathbf{u}_2, p_1, p_2) = \mathcal{L}_{\text{stab}}(\mathbf{w}_1, \mathbf{w}_2, q_1, q_2) \\
&\qquad \forall \left(\mathbf{w}_1(\mathbf{x}), \mathbf{w}_2(\mathbf{x})\right) \in \mathcal{W}_1 \times \mathcal{W}_2, (q_1(\mathbf{x}), q_2(\mathbf{x})) \in \mathcal{Q}
\end{aligned} \tag{A.15}$$

where the bilinear form and the linear functional are, respectively, defined as follows:

$$\begin{aligned}
\mathcal{B}_{\text{stab}}(\mathbf{w}_1, \mathbf{w}_2, q_1, q_2; \mathbf{u}_1, \mathbf{u}_2, p_1, p_2) &:= \mathcal{B}_{\text{Gal}}(\mathbf{w}_1, \mathbf{w}_2, q_1, q_2; \mathbf{u}_1, \mathbf{u}_2, p_1, p_2) \\
&-\frac{1}{2}\left(\mu \mathbf{K}_1^{-1} \mathbf{w}_1 - \text{grad}[q_1]; \frac{1}{\mu}\mathbf{K}_1 (\mu \mathbf{K}_1^{-1} \mathbf{u}_1 + \text{grad}[p_1]) \right) \\
&-\frac{1}{2}\left(\mu \mathbf{K}_2^{-1} \mathbf{w}_2 - \text{grad}[q_2]; \frac{1}{\mu}\mathbf{K}_2 (\mu \mathbf{K}_2^{-1} \mathbf{u}_2 + \text{grad}[p_2]) \right)
\end{aligned} \tag{A.16}$$

$$\mathcal{L}_{\text{stab}}(\mathbf{w}_1, \mathbf{w}_2, q_1, q_2) := \mathcal{L}_{\text{Gal}}(\mathbf{w}_1, \mathbf{w}_2, q_1, q_2) - \frac{1}{2}\left(\mu \mathbf{K}_1^{-1} \mathbf{w}_1 - \text{grad}[q_1]; \frac{1}{\mu}\mathbf{K}_1 \gamma \mathbf{b} \right)$$

$$-\frac{1}{2}\left(\mu\mathbf{K}_2^{-1}\mathbf{w}_2 - \text{grad}[q_2]; \frac{1}{\mu}\mathbf{K}_2\gamma\mathbf{b}\right) \tag{A.17}$$

It is important to note that the stabilization terms are residual-based. Moreover, the stabilization terms are of adjoint-type and are not of least-squares-type.

References

N. Aage, T. H. Poulsen, A. Gersborg-Hansen, and O. Sigmund. Topology optimization of large scale Stokes flow problems. *Structural and Multidisciplinary Optimization*, 35:175–180, 2008.

R. A. Adams and J. J. F. Fournier. *Sobolev Spaces*. Academic press, Oxford, U.K., 2003.

M. Ainsworth and J. T. Oden. A posteriori error estimation in finite element analysis. *Computer Methods in Applied Mechanics and Engineering*, 142:1–88, 1997.

C. Annavarapu, M. Hautefeuille, and J. E. Dolbow. A Nitsche stabilized finite element method for frictional sliding on embedded interfaces. Part I: single interface. *Computer Methods in Applied Mechanics and Engineering*, 268:417–436, 2014.

I. Babuška. The finite element method with Lagrangian multipliers. *Numerische Mathematik*, 20 (3):179–192, 1973.

I. Babuška and T. Strouboulis. *The Finite Element Method and its Reliability*. Oxford University Press, 2001.

I. Babuška, J. Whiteman, and T. Strouboulis. *Finite Elements: An Introduction to the Method and Error Estimation*. Oxford University Press, 2010.

S. Badia and R. Codina. Unified stabilized finite element formulations for the Stokes and the Darcy problems. *SIAM Journal on Numerical Analysis*, 47(3):1971–2000, 2009.

S. Badia and R. Codina. Stabilized continuous and discontinuous Galerkin techniques for Darcy flow. *Computer Methods in Applied Mechanics and Engineering*, 199(25):1654–1667, 2010.

C. Baiocchi, F. Brezzi, and L. Franca. Virtual bubbles and Galerkin-least-squares type methods (Ga.L.S.). *Computer Methods in Applied Mechanics and Engineering*, 105:125–141, 1993.

G. I. Barenblatt, I. P. Zheltov, and I. N. Kochina. Basic concepts in the theory of seepage of homogeneous liquids in fissured rocks [strata]. *Journal of Applied Mathematics and Mechanics*, 24:1286–1303, 1960.

Y. Bazilevs and T. J. R. Hughes. Weak imposition of Dirichlet boundary conditions in fluid mechanics. *Computers & Fluids*, 36(1):12–26, 2007.

R. Becker and R. Rannacher. An optimal control approach to a posteriori error estimation in finite element methods. *Acta Numerica 2001*, 10:1–102, 2001.

R. I. Borja and A. Koliji. On the effective stress in unsaturated porous continua with double porosity. *Journal of the Mechanics and Physics of Solids*, 57:1182–1193, 2009.

T. Borrvall and J. Petersson. Topology optimization of fluids in Stokes flow. *International Journal for Numerical Methods in Fluids*, 41:77–107, 2003.

S. C. Brenner and L. R. Scott. *The Mathematical Theory of Finite Element Methods*. Springer-Verlag, New York, USA, 1994.

F. Brezzi and M. Fortin. *Mixed and Hybrid Finite Element Methods, volume 15 of Springer series in computational mathematics*. Springer-Verlag, New York, 1991.

F. Brezzi, J. Douglas, and L. D. Marini. Two families of mixed elements for second order elliptic problems. *Numerische Mathematik*, 47:217–235, 1985.

F. Brezzi, J. Douglas, R. Durran, and L. D. Marini. Mixed finite elements for second order elliptic problems in three variables. *Numerische Mathematik*, 51:237–250, 1987.

F. Brezzi, D. Boffi, L L. Demkowicz, R. G. Durán, R. S. Falk, and M. Fortin. *Mixed Finite Elements, Compatibility Conditions, and Applications*. Springer, New York, 2008.

A. N. Brooks and T. J. R. Hughes. Streamline upwind/Petrov-Galerkin formulations for convection dominated flows with particular emphasis on the incompressible Navier-Stokes equations. *Computer Methods in Applied Mechanics and Engineering*, 32(1-3):199–259, 1982.

V. J. Challis and J. K. Guest. Level set topology optimization of fluids in Stokes flow. *International Journal for Numerical Methods in Engineering*, 79:1284–1308, 2009.

J. Chang, K. B. Nakshatrala, and J. N. Reddy. Modification to Darcy-Forchheimer model due to pressure-dependent viscosity: consequences and numerical solutions. *Journal of Porous Media*, 20:263–285, 2017.

C. Y. Chen and E. Meiburg. Miscible porous media displacements in the quarter five-spot configuration. Part 1. The homogeneous case. *Journal of Fluid Mechanics*, 371:233–268, 1998a.

C. Y. Chen and E. Meiburg. Miscible porous media displacements in the quarter five-spot configuration. Part 2. Effect of heterogeneities. *Journal of Fluid Mechanics*, 371:269–299, 1998b.

J. Choo and R. I. Borja. Stabilized mixed finite elements for deformable porous media with double porosity. *Computer Methods in Applied Mechanics and Engineering*, 293:131–154, 2015.

J. Choo, J. White, and R. I. Borja. Hydromechanical modeling of unsaturated flow in double porosity media. *International Journal of Geomechanic*, 2015.

R. L. Chuoke, P. Van Meurs, and C. van der Poel. The instability of slow, immiscible, viscous liquid-liquid displacements in permeable media. *AIME MET SOC TRANS*, 216:188–194, 1959.

A. Embar, J. Dolbow, and I. Harari. Imposing Dirichlet boundary conditions with Nitsche's method and spline-based finite elements. *International Journal for Numerical Methods in Engineering*, 83:877–898, 2010.

L. C. Evans. *Partial Differential Equations*. American Mathematical Society, Providence, 1998.

L. P. Franca and T. J. R. Hughes. Two classes of mixed finite element methods. *Computer Methods in Applied Mechanics and Engineering*, 69:89–129, 1988.

M. E. Gurtin. *An Introduction to Continuum Mechanics*. Academic Press, Inc., New York, 1981.

E. Hairer, S. P. Norsett, and G. Wanner. *Solving Ordinary Differential Equations I: Nonstiff Problems*. Springer-Verlag, New York, USA, 1993.

P. Hansbo. Nitsche's method for interface problems in computational mechanics. *GAMM-Mitteilungen*, 28:183–206, 2005.

M. T. Heath. *Scientific Computing*. McGraw-Hill, New York, 2001.

N. J. Higham. *Accuracy and Stability of Numerical Algorithms*. SIAM, Philadelphia, second edition, 2002.

G. M. Homsy. Viscous fingering in porous media. *Annual Review of Fluid Mechanics*, 19:271–311, 1987.

T. J. R. Hughes. *The Finite Element Method: Linear Static and Dynamic Finite Element Analysis*. Prentice-Hall, Englewood Cliffs, New Jersey, USA, 1987.

T. J. R. Hughes. Multiscale phenomena: Green's functions, the Dirichlet-to-Neumann formulation, subgrid scale models, bubbles and the origins of stabilized methods. *Computer Methods in Applied Mechanics and Engineering*, 127:387–401, 1995.

T. J. R. Hughes, L. Mazzei, and K. E. Jansen. Large eddy simulation and the variational multiscale method. *Computing and Visualization in Science*, 3(1):47–59, 2000.

T. J. R. Hughes, G. Scovazzi, and L. P. Franca. Multiscale and stabilized methods. *Encyclopedia of Computational Mechanics*, 2004.

T. J. R. Hughes, A. Masud, and J. Wan. A stabilized mixed discontinuous Galerkin method for Darcy flow. *Computer Methods in Applied Mechanics and Engineering*, 195:3347–3381, 2006.

J. K. Hunter and B. Nachtergaele. *Applied Analysis*. World Scientific, New Jersey, 2001.

A. Masud and T. J. R. Hughes. A stabilized mixed finite element method for Darcy flow. *Computer Methods in Applied Mechanics and Engineering*, 191:4341–4370, 2002.

C. E. Mongan. Validity of Darcy's law under transient conditions. Technical report, U.S. Geological Survey Professional Paper 1331, 1985.

M. K. Mudunuru and K. B. Nakshatrala. On enforcing maximum principles and achieving element-wise species balance for advection–diffusion–reaction equations under the finite element method. *Journal of Computational Physics*, 305:448–493, 2016.

H. Nagarajan and K. B. Nakshatrala. Enforcing the non-negativity constraint and maximum principles for diffusion with decay on general computational grids. *International Journal for Numerical Methods in Fluids*, 67(7):820–847, 2011.

K. B. Nakshatrala and K. R. Rajagopal. A numerical study of fluids with pressure-dependent viscosity flowing through a rigid porous medium. *International Journal for Numerical Methods in Fluids*, 67:342–368, 2011.

K. B. Nakshatrala, D. Z. Turner, K. D. Hjelmstad, and A. Masud. A stabilized mixed finite element formulation for Darcy flow based on a multiscale decomposition of the solution. *Computer Methods in Applied Mechanics and Engineering*, 195:4036–4049, 2006.

K. B. Nakshatrala, S. H. S. Joodat, and R. Ballarini. Modeling flow in porous media with double porosity/permeability: Mathematical model, properties, and analytical solutions. *arXiv preprint arXiv:1605.07658*, 2016.

J. Nitsche. Über ein Variationsprinzip zur Lösung von Dirichlet-Problemen bei Verwendung von Teilräumen, die keinen Randbedingungen unterworfen sind. In *Abhandlungen aus dem mathematischen Seminar der Universität Hamburg*, volume 36, pages 9–15. Springer, 1971.

G. Pacquaut, J. Bruchon, N. Moulin, and S. Drapier. Combining a level-set method and a mixed stabilized P1/P1 formulation for coupling Stokes–Darcy flows. *International Journal for Numerical Methods in Fluids*, 69:459–480, 2012.

K. R. Rajagopal. On a hierarchy of approximate models for flows of incompressible fluids through porous solids. *Mathematical Models and Methods in Applied Sciences*, 17(02):215–252, 2007.

P. A. Raviart and J. M. Thomas. A mixed finite element method for 2nd order elliptic problems. In *Mathematical Aspects of the Finite Element Method*, pages 292–315, Springer, New York, 1977.

E. Rothe. Zweidimensionale parabolische randwertaufgaben als grenzfall eindimensionaler randwertaufgaben. *Mathematische Annalen*, 102:650–670, 1930.

P. G. Saffman and G. Taylor. The penetration of a fluid into a porous medium or Hele-Shaw cell containing a more viscous liquid. *Proceedings of the Royal Society of London A: Mathematical, Physical and Engineering Sciences*, 245:312–329, 1958.

D. Schillinger, I. Harari, M. C. Hsu, D. Kamensky, S. K. F. Stoter, Y. Yue, and Y. Zhao. The non-symmetric Nitsche method for the parameter-free imposition of weak boundary and coupling

conditions in immersed finite elements. *Computer Methods in Applied Mechanics and Engineering*, 309:625–652, 2016.

M. Shabouei. *Theoretical and numerical study in porous media: Solution verification and viscous fingering instability.* PhD thesis, University of Houston, Houston, Texas, August 2016.

M. Shabouei and K. B. Nakshatrala. Effect of temperature and numerical stabilization on viscous fingering and mixing. *Under preparation.*

M. Shabouei and K. B. Nakshatrala. Mechanics-based solution verification for porous media models. *Communications in Computational Physics*, 20:1127–1162, 2016.

F. I. Stalkup. *Miscible displacement.* Society of Petroleum Engineers, 1983.

S. R. Stock. *Microcomputed Tomography: Methodology and Applications.* CRC Press, Boca Raton, 2008.

D. Z. Turner, K. B. Nakshatrala, and K. D. Hjelmstad. On the stability of bubble functions and a stabilized mixed finite element formulation for the Stokes problem. *International Journal for Numerical Methods in Fluids*, 60:1291–1314, 2009.

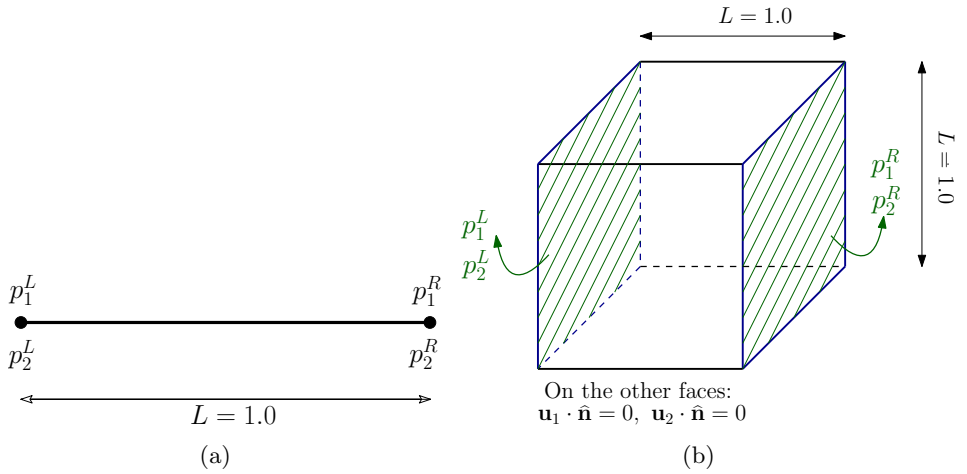


FIGURE 1. Patch tests: The left figure provides a pictorial description of the 1D patch test and the right one shows the domain and the boundary conditions in 3D patch test. In 3D test, pressures are prescribed on the left and right faces and on the other faces, the normal component of velocity is zero in both pore-networks.

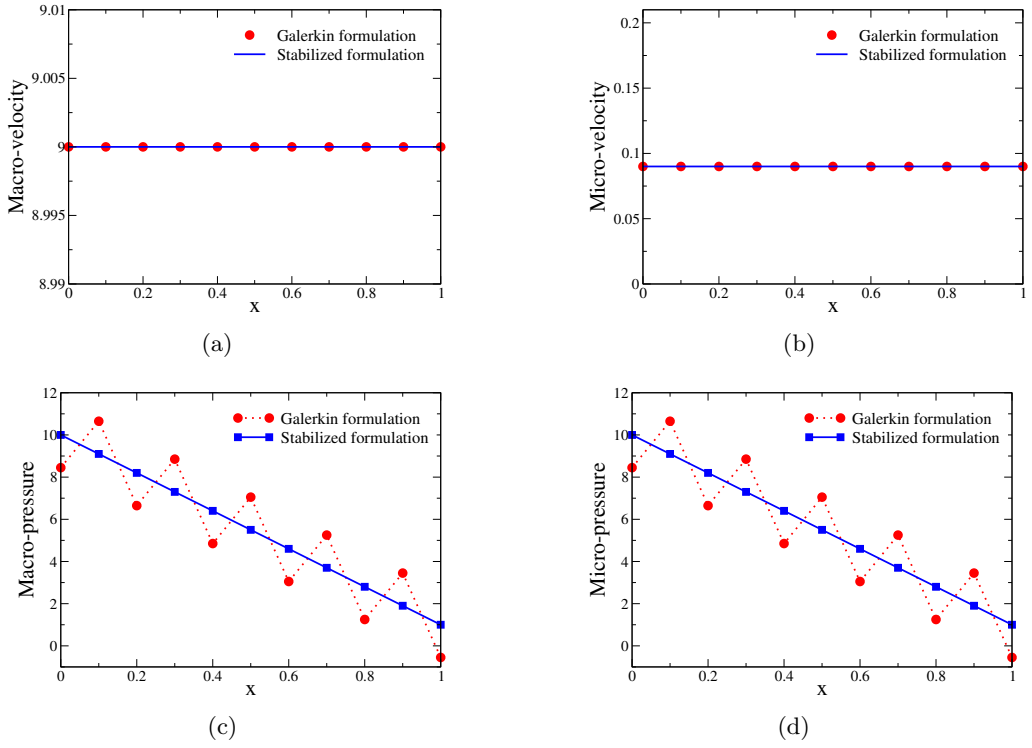
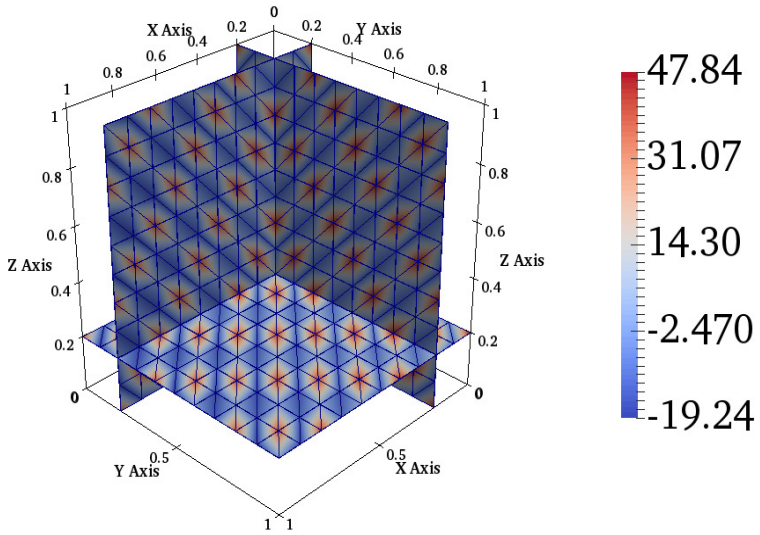
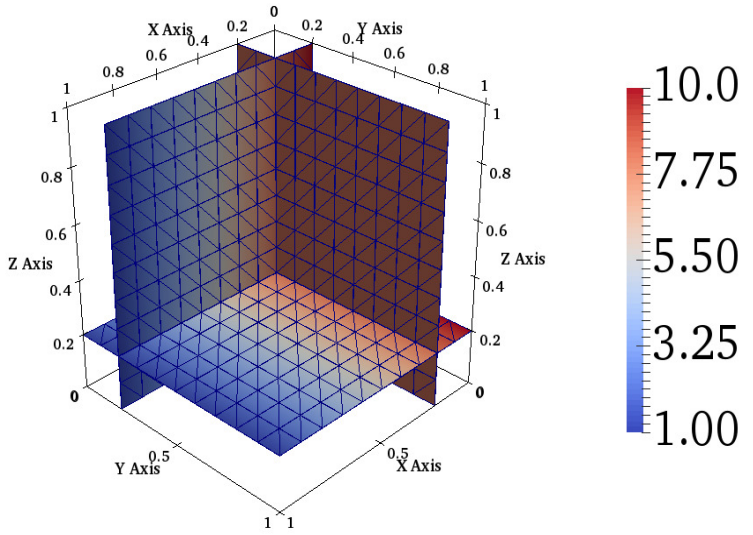


FIGURE 2. 1D patch test: Pressure and velocity in pore-networks under Galerkin and proposed formulations. For velocity fields, the values match with the analytical solution up-to machine precision under both formulations. For pressure fields, spurious oscillations are observed under Galerkin formulation, even for equal-order interpolation. Under stabilized mixed formulation, such oscillations are eliminated.



Pressure under Galerkin formulation



Pressure under proposed stabilized formulation

FIGURE 3. 3D patch test: Pressure profiles in the micro-pores and macro-pores in 3D constant flow patch test under Galerkin and the proposed stabilized mixed formulations. Under Galerkin formulation, spurious oscillations are observed in pressure fields, even for equal-order interpolation, which implies that the results are unstable. Such oscillations are eliminated from the pressure profiles under the proposed mixed formulation.

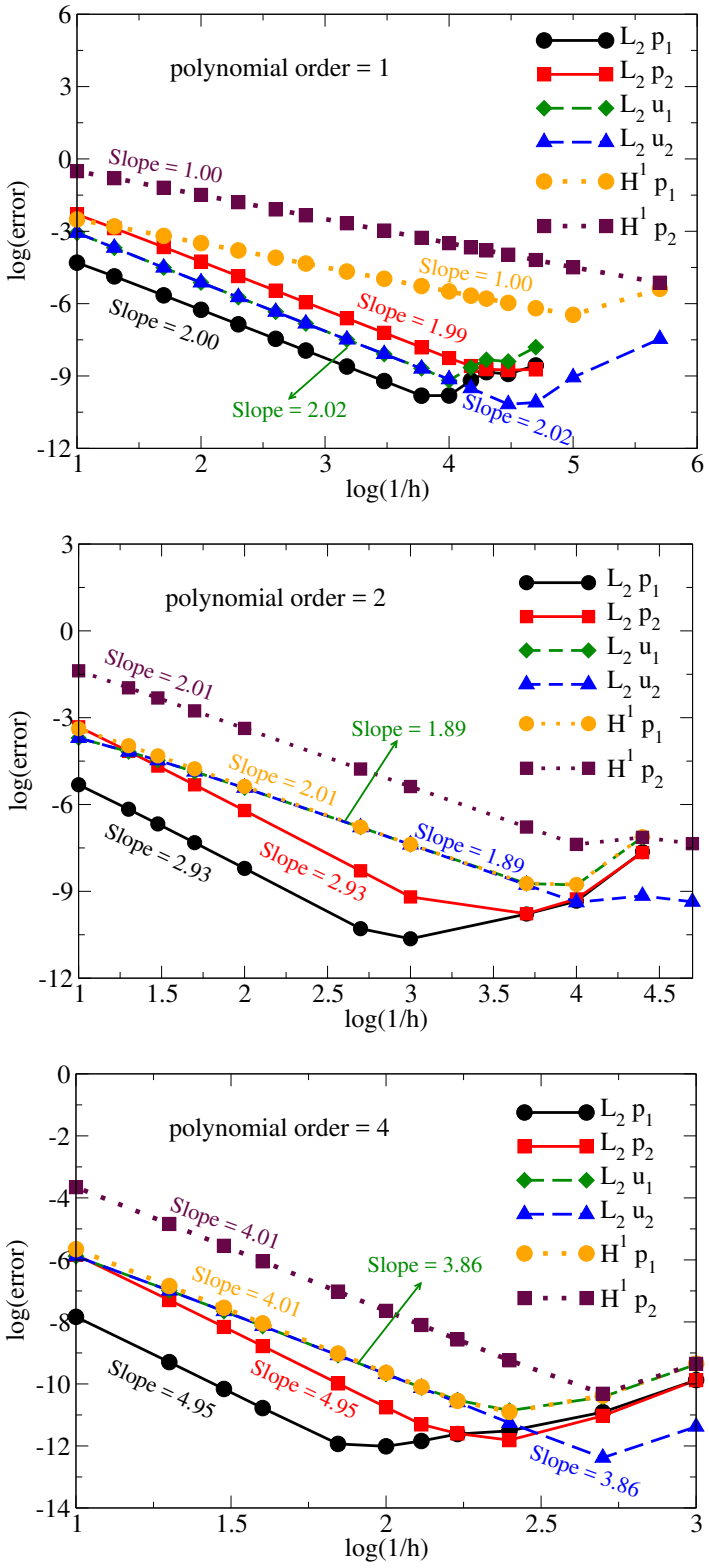


FIGURE 4. 1D numerical convergence analysis: This figure illustrates the numerical convergence of the proposed stabilized mixed formulation under h-refinement for various polynomial orders. The rate of convergence is polynomial, which is in accordance with the theory.

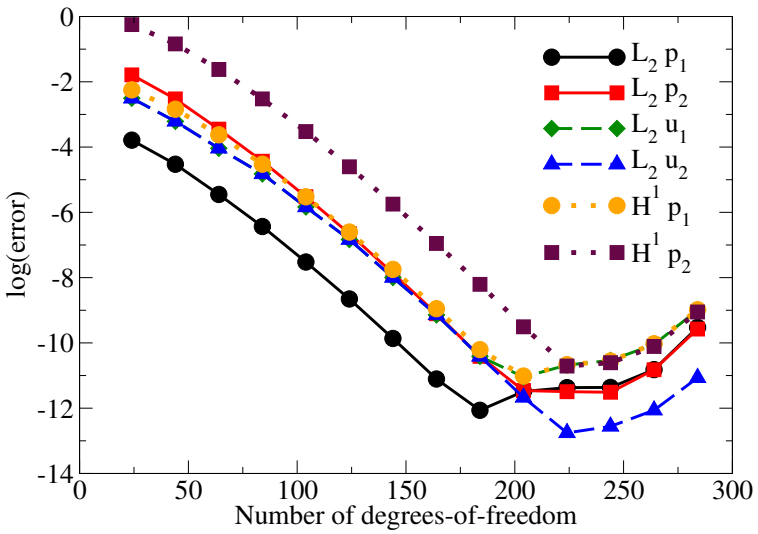


FIGURE 5. 1D numerical convergence analysis: This figure illustrates the numerical convergence of the proposed stabilized mixed formulation under p-refinement for a fixed mesh size ($h = 0.2$). The number of degrees-of-freedom corresponds to $p = 1$ to 14. The rate of convergence is exponential, which is in accordance with the theory.

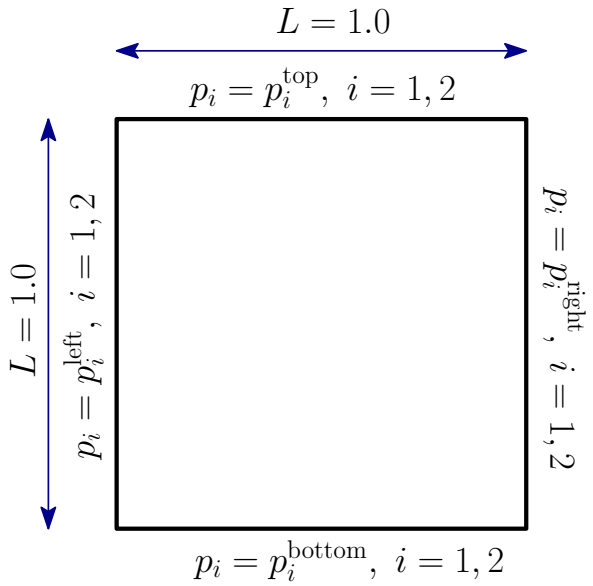


FIGURE 6. 2D numerical convergence analysis: This figure provides a pictorial description of the boundary value problem employed in the 2D numerical convergence analysis.

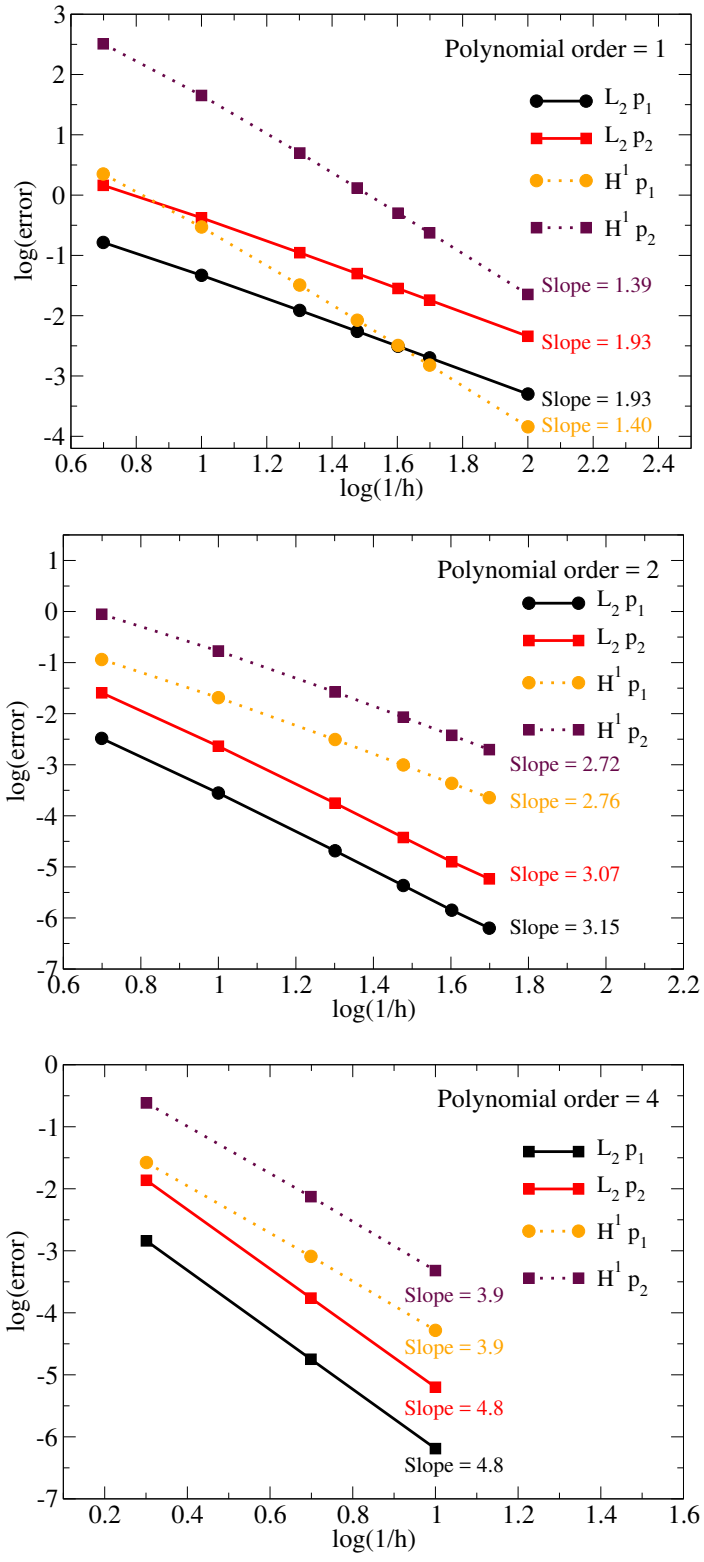


FIGURE 7. 2D numerical convergence analysis: This figure shows the numerical convergence under h-refinement for various polynomial orders. The rate of convergence is polynomial, which is in accordance with the theory.

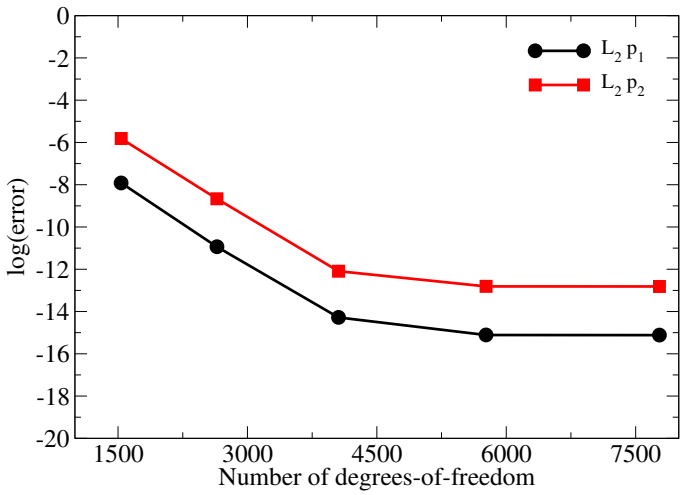


FIGURE 8. 2D numerical convergence analysis: This figure shows the numerical convergence under p-refinement for a fixed mesh size ($h = 0.2$). The number of degrees-of-freedom corresponds to $p = 3$ to 7. The rate of convergence is exponential, which is in accordance with the theory. Note that the error flattened out around 10^{-16} for larger number of degrees-of-freedom. This is expected as the machine precision on a 64-bit machine is around 10^{-16}.

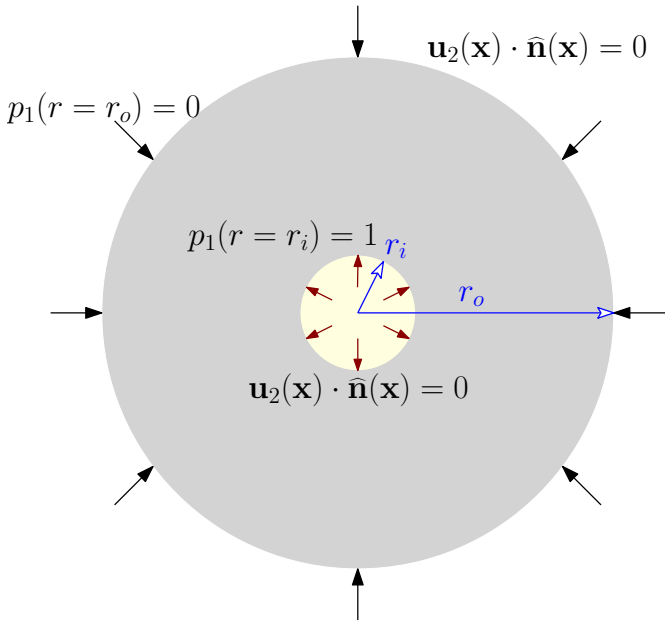
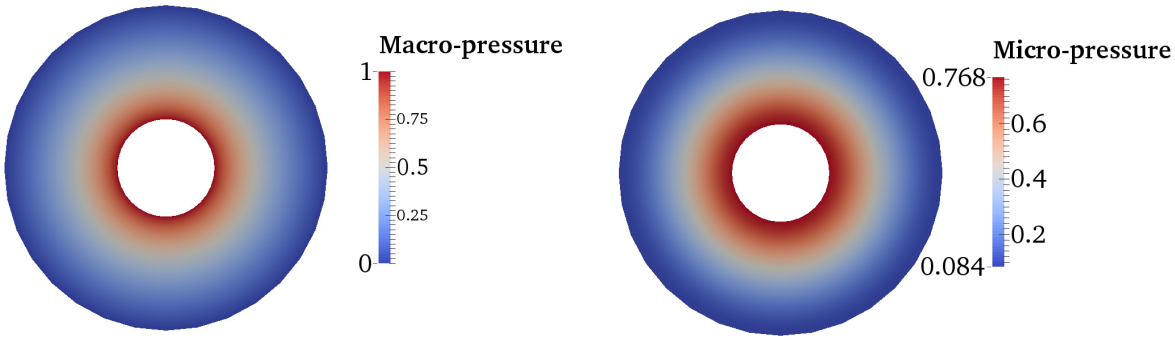
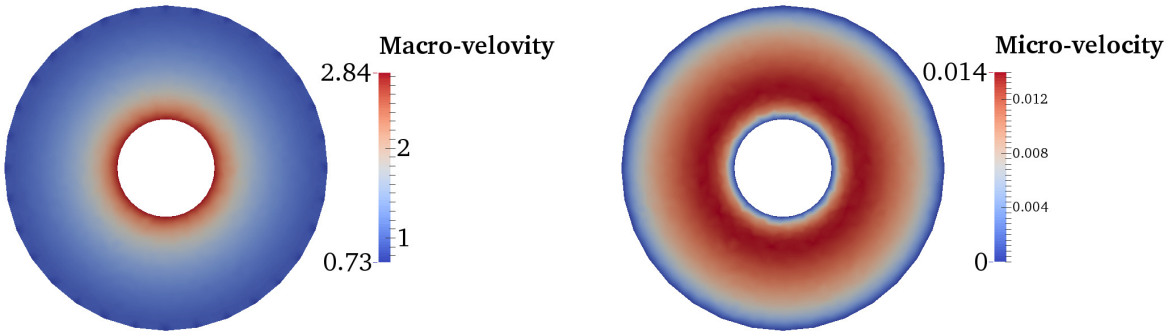


FIGURE 9. Two-dimensional candle filter problem: This figure provides a pictorial description of the candle filter problem which is used to study weak enforcement of velocity boundary conditions. There is no discharge on the inner and outer surfaces of the micro-pore network. For the macro-pore network, the inner surface is subjected to a pressure of unity, and the outer surface is subjected to zero pressure.

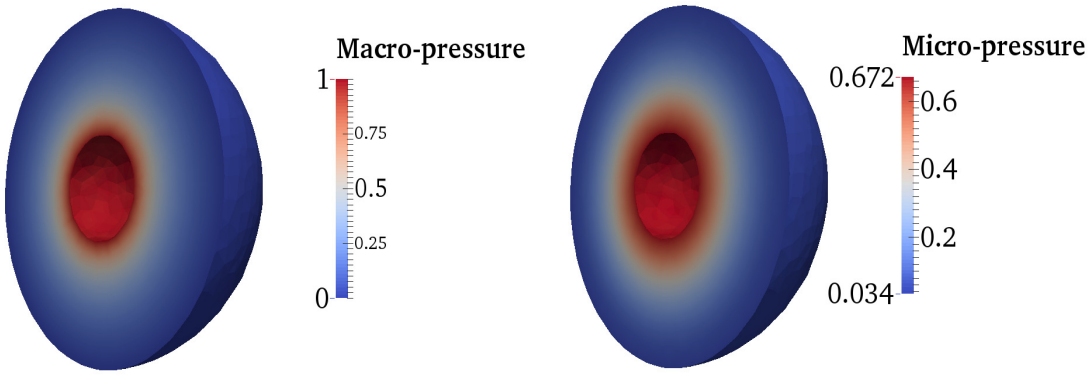


(a) Pressure fields

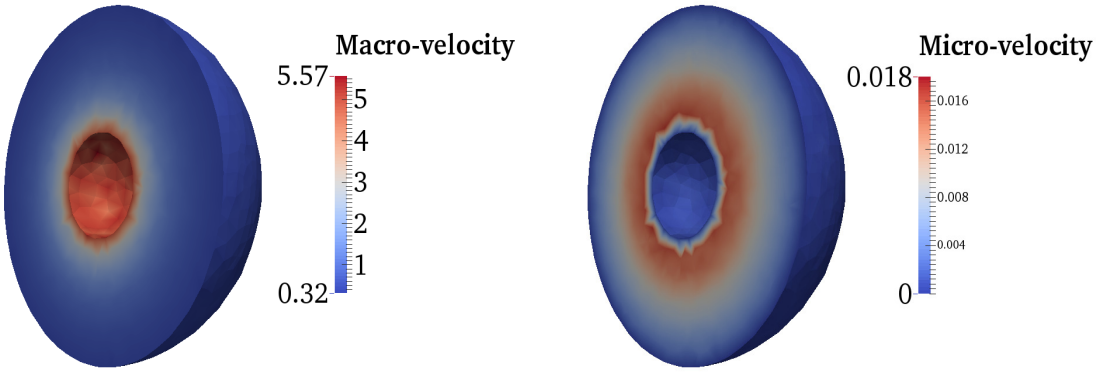


(b) Velocity vector fields

FIGURE 10. Two-dimensional candle filter problem: This figure shows the contours of pressures and velocities in macro- and micro-pore networks under the extended framework for weak enforcement of velocity boundary conditions. Although there is no discharge from the micro-pore network on the boundary, there is discharge in the micro-pore network within the domain.



(a) Pressure fields



(b) Velocity vector fields

FIGURE 11. Three-dimensional hollow sphere problem: This figure shows the contours of pressures and velocities in the two pore-networks under the extended framework for weak enforcement of velocity boundary conditions. On the inner and outer surfaces, pressure is prescribed for the macro-pore network while there is no discharge for the micro-pore network. Although there is no discharge from the micro-pore network on the boundary, there is discharge in the micro-pore network within the domain.

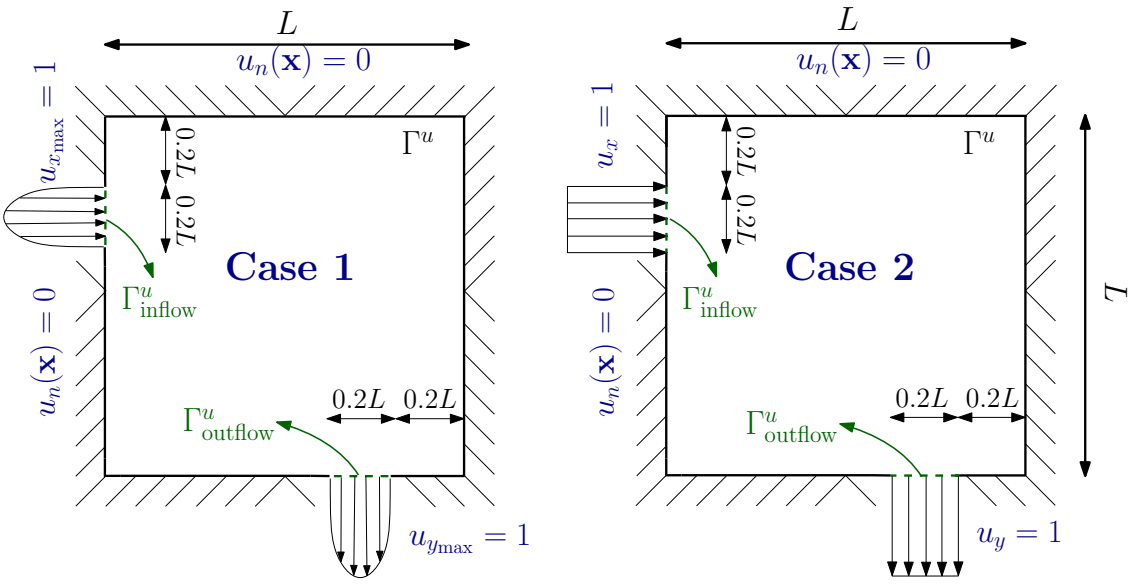
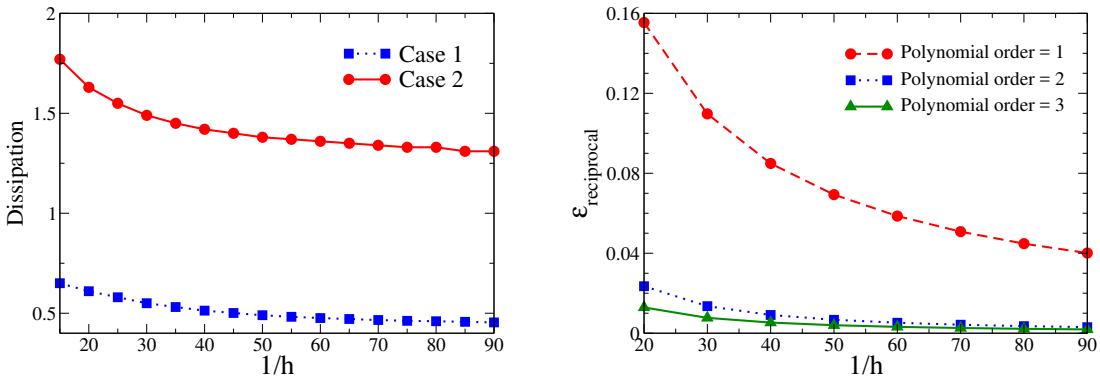


FIGURE 12. Pipe bend problem: In case 1, for the macro-pore network, an inflow parabolic velocity is enforced on Γ^u_{inflow} while an outflow parabolic velocity is applied on $\Gamma^u_{\text{outflow}}$. In case 2, an inflow constant velocity is enforced on Γ^u_{inflow} while an outflow constant velocity is applied on $\Gamma^u_{\text{outflow}}$ for the macro-pore network. On the other parts of the boundary, normal component of velocity is assumed to be zero.



(a) Dissipation

(b) Error in reciprocal relation

FIGURE 13. Pipe bend problem: The left figure shows the variation of dissipation with mesh refinement for both cases shown in figure 12. As can be seen, the dissipation decreases monotonically with mesh refinement which is in accordance with the theory for this problem. The right figure, shows the variation of $\varepsilon_{\text{reciprocal}}$ with mesh refinement using the two cases for different orders of interpolation. The numerical error in the reciprocal relation decreases monotonically with mesh refinement for this test problem which shows the monotonic convergence of numerical solutions.

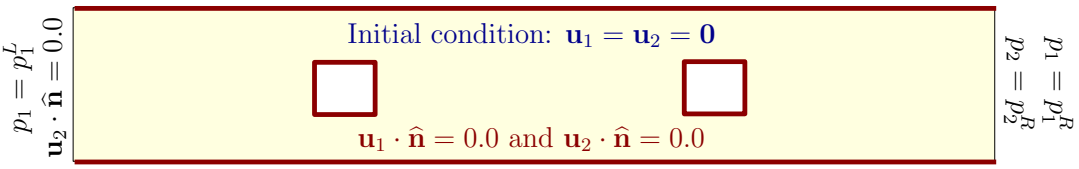


FIGURE 14. Transient 2D flow problem: This figure shows the computational domain, initial and boundary conditions for the transient problem.

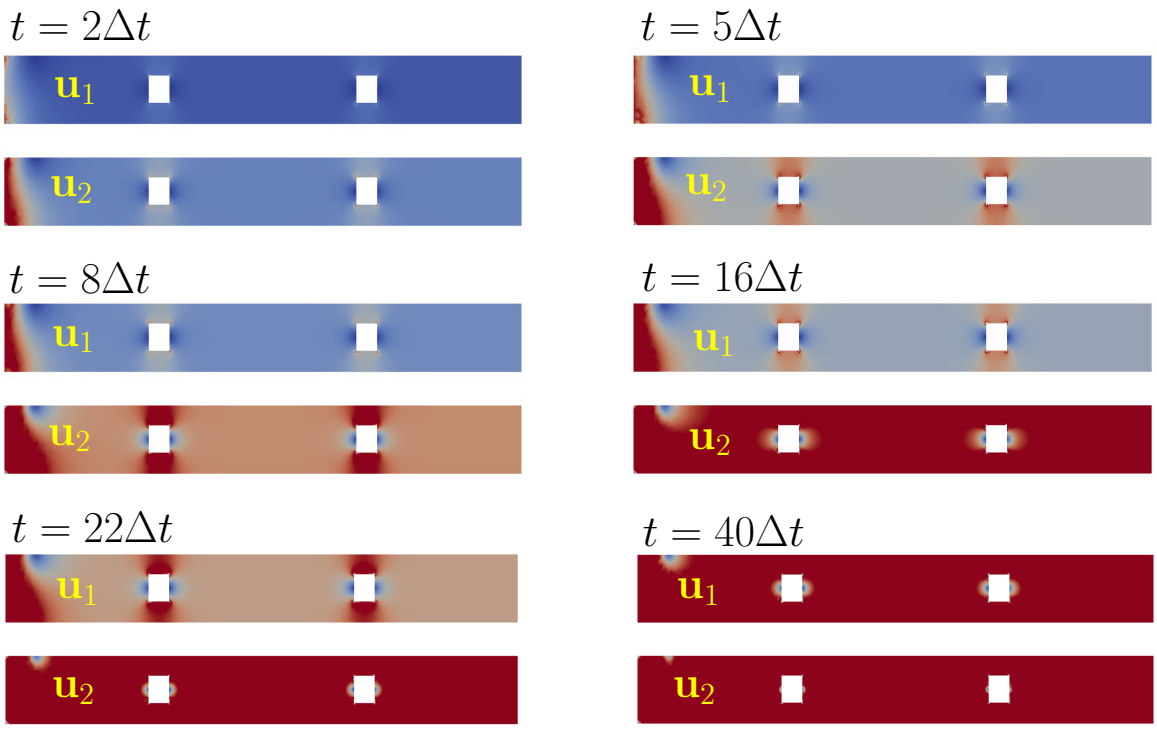


FIGURE 15. Transient 2D flow problem: This figure shows a comparison between macro- and micro-velocities at different time steps. As can be seen, the rate of decay of the solution in the macro-pore network is slower than that of the micro-pore network which is due to the higher permeability of the macro-pore network. Hence, the micro-velocity reaches the steady state faster than the macro-velocity.

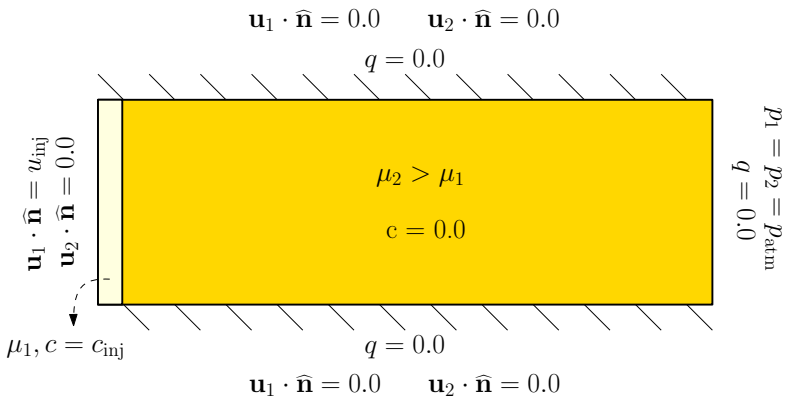


FIGURE 16. Hele-Shaw cell: This figure shows the pictorial description of the coupled flow-transport problem including initial and boundary conditions.

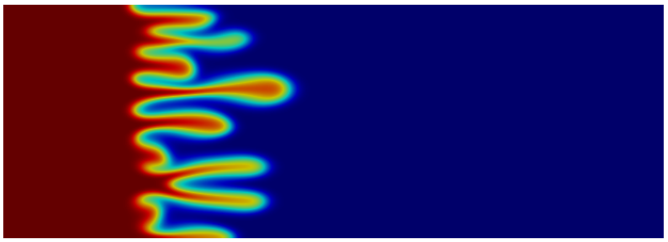


FIGURE 17. Coupled flow-transport problem: This figure shows that Saffman-Taylor-type physical instabilities can also occur in a porous domain exhibiting double porosity/permeability. As can be seen, the proposed stabilized formulation is capable of eliminating the spurious numerical instabilities without suppressing the underlying physical instability.